TECHNICAL NOTE

D-829

CALCULATED NORMAL LOAD FACTORS ON LIGHT AIRPLANES TRAVERSING THE TRAILING VORTICES OF HEAVY TRANSPORT AIRPLANES

By William A. McGowan

Langley Research Center
Langley Field, Va.

NATIONAL AERONAUTICS AND SPACE ADMINISTRATION

WASHINGTON

May 1961

NATIONAL AERONAUTICS AND SPACE ADMINISTRATION

TECHNICAL NOTE D-829

CALCULATED NORMAL LOAD FACTORS ON LIGHT AIRPLANES TRAVERSING THE TRAILING VORTICES OF HEAVY TRANSPORT AIRPLANES

By William A. McGowan

SUMMARY

Results are presented of normal-load-factor calculations made for a light normal-category airplane and a light transport-category airplane traversing the trailing vortices generated by each of three heavy transport airplanes. With each light airplane, the normal load factors were determined for several penetration paths lying in a plane perpendicular to the trailing vortices and for three center-of-gravity locations and velocities. Also determined for the light normal-category airplane were the elevator deflection required to maintain 1 g flight and the vertical displacements of the airplane from the prescribed penetration paths while traversing the vortices.

The methods used (formulated from available theories) and an example illustrating use of derived charts for computing normal load factors are given in the appendixes.

The results indicate that light airplanes traversing the wakes of currently operational heavy transport airplanes can experience loading conditions that exceed the design limit and, in some cases, the design ultimate load factors. For light airplanes traversing the wake generated by a proposed supersonic transport airplane the design ultimate load factors can be greatly exceeded. It was also shown that load factors imposed by the vortex system could be alleviated by elevator deflection; however, because of inherent pilot and control-system lag, the load factors would almost certainly be aggravated rather than alleviated.

INTRODUCTION

The adverse effects on an airplane traversing the wake of another airplane are well known (see, for example, refs. 1 to 4) and a number of papers have been written which bear on various phases of the problem

(for example, refs. 5 to 8). As a result of these works, it is known that the vortex trails can persist for a minute or more under calm atmospheric conditions and are rapidly broken up by turbulence and that there is good agreement between the measured and the calculated intensity of trailing vortices. Also, these investigations reveal certain trends from which it can be reasoned qualitatively that (1) since the vortex trails are invisible no appropriate evasive action can be taken by the pilot except to be alert on calm days in high-intensity traffic areas whether or not another airplane is in sight, (2) reducing speed or flying either above or below the path of an airplane should reduce the magnitude of the load factors, (3) either entering perpendicular to or quartering the vortex trails will result in approximately the same magnitude of load factors except as such maneuvers might cause the period of the vortex impulses to coincide more nearly with the natural oscillations of the airplane, and (4) the effect of elevator motion on the load factors could either be canceling or aggravating, depending upon the phasing of the elevator motion with the impulses from the vortices.

Although these factors and trends are known, very little information is available on either the actual quantities involved or a reasonably simple method for computing the load factors in a given case. Therefore, it is the purpose of this report to present the results of a series of systematic normal-load-factor calculations and to present the methods used. The calculations were made for a light normal-category airplane and a light transport-category airplane traversing, under various conditions, the wakes generated by each of three heavy transport airplanes.

A list of the symbols used throughout the paper is given in appendix A.

SCOPE OF CALCULATIONS

The variables involved in this normal-load-factor investigation are contingent upon (1) the characteristics and flight conditions of the generating airplanes and (2) the velocity, static stability, penetration path, configuration, and elevator motion of the penetrating airplanes.

The three heavy transport airplanes generating the wakes are referred to as the generating airplanes. The two light airplanes penetrating the wakes of the heavy airplanes are referred to as the penetrating airplanes. Three-view sketches of the penetrating airplanes are given in figure 1.

Generating Airplanes

The characteristics of the generating airplanes required to establish, by theoretical means, the strength and behavior of the wing-tip trailing vortices are given in table I. Two of the three transport airplanes selected, a military transport G_A and a swept-wing civil transport G_B, are presently operational and the third airplane G_C represents a proposed supersonic transport of the future (ref. 9). Three generating airplanes were selected so that the relative effects of airplane geometry and weight on the normal load factors experienced by a penetrating airplane could be determined. The flight conditions are those that might exist shortly before landing or after take-off, as the probability of one airplane's traversing the wake of another would be greatest near airfields where the relative intensity of airplane traffic is high.

A schematic sketch of the wing-tip rolled-up trailing vortices shed by the generating airplanes is shown in figure 2. The generating airplanes were considered to be flying straight and level for the present analysis.

Penetrating Airplanes

Airplane P_A is a typical light normal-category airplane of about 2,000 pounds with externally braced high wing and single engine. Airplane P_B is a light transport-category airplane in current use. (See fig. 1.) The geometric and aerodynamic characteristics pertinent to the analysis are listed in table II. The aerodynamic characteristics were obtained from either available methods or suggested values presented in the literature.

Airplane P_A was considered to meet standards for normal-category aircraft as defined in reference 10. Airplanes in this category are intended for nonacrobatic operation. The positive and negative design limit load factors are 3.8 and -1.5, respectively. The limit load factors represent the maximum loads anticipated in service. The airplane structure is, however, designed to support ultimate loads of magnitudes $1\frac{1}{2}$ times the limit loads. The positive and negative ultimate load factors are, therefore, 5.7 and -2.25, respectively.

Airplane P_B, in the transport category, was considered to comply with the requirements of reference 11. The positive and negative design limit load factors are 2.5 and -1.0, respectively, and the corresponding ultimate load factors are 3.75 and -1.5.

The penetrating airplanes, prior to entering the trailing vortices of the generating airplanes, are trimmed for flight along the prescribed penetration paths. All the penetration paths are in the plane shown in figure 2. The plane of the paths is perpendicular to the trailing vortices of the generating airplane. The line of vortex centers, noted in figure 2, is the reference line used in designating the level and inclination of the penetration paths. An illustrative sketch of the various paths through the vortices is shown in figure 3.

Although the altitude along the penetration paths varies, the mass density of air is assumed to be constant at a value of 0.002309 slug per cubic foot, occurring at the pressure altitude of 1,000 feet. For consistency of calculations, the penetrating airplanes enter the vortices from the left, as indicated in figure 3. The flight conditions for the penetrating airplanes are enumerated in table III as cases 1 to 16.

The effects of penetrating-airplane velocity, center-of-gravity location (static stability), penetration path, configuration, and vortex intensity on the normal load factor were determined from the load-factor time histories calculated for cases 1 to 14 by varying the aforementioned variables in a systematic manner. The elevator of the penetrating airplane was held fixed during evaluation of these effects.

The additional influence of an estimated elevator motion on the load factor of a penetrating airplane was determined as case 15. The elevator motion represented an attempt by the pilot to alleviate the normal load factors imposed by the vortices. Corrective pitch action (down elevator) was initiated as the penetrating airplane experienced the positive load factors upon first entering the vortex system. The estimated control motion was made consistent with what were believed to be reasonable control rates and pilot and control-system lag.

In addition, calculations were made to evaluate the incremental elevator motion required to maintain 1 g flight while traversing the vortices (case 16). Also, vertical displacements of the airplane from a prescribed penetration path through the vortices were determined for cases 1, 2, and 3.

METHODS AND RESULTS

As defined in this paper, the normal load factor on an airplane traversing trailing vortices is composed of the increments related to steady-state flight, vortex flow, and airplane dynamic response in pitch due to the vortex flow and/or incremental elevator deflection. The airplane is considered to traverse the vortices in such a way that the component loads induced are symmetrical about its center line and its

response is in the vertical plane only. The methods for calculating the vortex strength and normal load factors make use of various established theories. Details of the methods used are presented in appendix B.

Trailing Vortices

In order to evaluate the normal-load-factor increments related to the vortex flow and the airplane pitch response (motivated by the vortex flow), it is first necessary to determine the intensity and behavior of the vortices.

In accordance with theoretical expressions given in reference 12, and in conjunction with the geometric characteristics and flight conditions of the generating airplanes, the vortex parameters were evaluated for a distance e behind the wing at which the wing-tip trailing vortices became essentially rolled up. These parameters are: (1) the vortex-core radius r_c, (2) the tangential velocity w_v of the circulatory flow in the plane of the penetration paths (example shown in fig. 4), (3) the distance d between the core centers, (4) the distance x from the nearest vortex core where the airplane is considered to first penetrate the vortices, and (5) the downward velocity of the vortex cores w_d with reference to the generating airplane's flight path. These vortex parameters define the intensity, velocity distribution, location, and movement of the trailing vortices for the generating airplanes and are given in table IV.

The theoretical expressions indicate that the tangential velocity approaches infinity near the vortex center. However, in this paper the vortex core is assumed to rotate as a solid body; hence, the velocity within the core decreases linearly from a maximum at the periphery to zero at the center.

Normal Load Factor

The normal load factor on the penetrating airplanes traversing the vortex fields can be written

$$n = n_1 + n_l + n_r \tag{1}$$

where n_1 represents the trim steady-state or datum load factor, n_l represents the load factor related to the vortex-system velocity, and n_r represents the load factor due to airplane motion or dynamic response about the penetration path. Equation (1) can be written in coefficient form as

$$n = 1 + \left(\frac{dC_L}{d\alpha}\frac{qS}{W}\right)_p(\alpha_l + \alpha_r) \qquad (2)$$

The vortex-induced angle of attack on the penetrating airplane α_l was found by determining the ratio (angle) of the resultant vortex-system velocity component (perpendicular to the penetration path) to the forward velocity of the penetrating airplane and then adjusting this ratio (angle) for lag-in-lift effect. An example of the resultant vortex-system velocity component for case 2 is shown in figure 5. The induced angle of attack α_r due to airplane response about the penetration path was evaluated from the second-order differential equation for the longitudinal motion of an assumed rigid penetrating airplane with impressed moment caused by the vortex flow and/or elevator motion. The values of the other parameters in equation (2) are listed in table II. Equation (2) was solved for n at times selected along the penetration paths to represent adequately the normal-load-factor time histories. Typical normal load factors n_1, n_l, and n_r and the sum of these factors calculated for an elevator-fixed penetration case are shown in figure 6.

Plotted time-history results are shown in figure 7 for the calculated normal load factors on airplane P_A traversing with elevator fixed the vortices of airplane G_A. The time histories are grouped to illustrate the effects of velocity (fig. 7(a)), center-of-gravity location (fig. 7(b)), height of penetration path with respect to the line of vortex centers (fig. 7(c)), and angle of penetration with respect to the line of vortex centers (fig. 7(d)). In figures 8 and 9 the normal-load-factor time histories are presented for airplanes P_A and P_B, respectively, when penetrating with elevator fixed the vortices of airplanes G_A, G_B, and G_C. The effect of an estimated elevator motion on penetrating airplane P_A is shown in figure 10. Also shown in the figure is the time history of the estimated elevator motion. In addition, the time history of the initial incremental elevator deflection required for 1 g flight through the vortices is indicated. The limit and ultimate design load factors for the penetrating airplanes are indicated in figures 8, 9, and 10.

The elevator deflection required for 1 g flight was defined as the deflection necessary to maintain the normal load factor at the 1 g datum value and is expressed by a relation developed from the second-order differential equation for the longitudinal motion of the penetrating airplane. An example of the load factor induced by the vortices (elevator fixed) and the calculated elevator deflection required to maintain 1 g flight in this example are shown in figure 11.

Vertical Displacement

The vertical displacements of airplane P_A from prescribed penetration paths were determined by numerically integrating, twice with respect to time, the normal acceleration (from 1 g flight) calculated for the airplane with elevator fixed. Vertical displacements of the penetrating airplane, as determined for several cases, are plotted in figure 12.

DISCUSSION

The discussion on the theoretical behavior of the trailing vortices is followed by accounts of the effects of certain variables on the normal load factors, the elevator requirement for 1 g flight through the vortices, and vertical displacements from the prescribed penetration paths.

Trailing Vortices

The vortices become essentially rolled up at specific distances behind the wings as listed in table IV. At these distances and beyond, the disturbances caused by the propeller and/or jet-engine-exhaust wakes were assumed to be negligible. The flight-test results of references 5 and 6 indicate that this was a reasonable assumption. The magnitude and distribution of the resultant velocities of the trailing vortices as calculated in this report were found to be comparable to flight measurements given in reference 5.

The flight-test results (refs. 5, 6, and 7) also show that the rolled-up vortices can maintain approximately initial strength for 30 seconds and up to possibly a minute or more in very calm air. No dissipation of vortex strength was considered because of the slow rate of decay of the vortices. Therefore the assumption was made that the spanwise wing loading was symmetrical for an airplane penetrating the vortices perpendicular to the vortex trail. Small amounts of atmospheric turbulence can, however, cause the vortices to move erratically and decay rapidly (refs. 5 and 8). The circulatory velocity contours of the vortices were calculated from equations derived for wings having an elliptical spanwise loading. These equations would be applicable for wings having near elliptical loading either with or without flap deflections provided the flaps are full span. If the flaps are partial span, and deflected, the spanwise loading distributions would probably not be elliptical in shape. It is possible, then, that more than two rolled-up vortices could be developed rearward of each wing.

The behavior of the trailing vortices behind wings having abrupt changes in spanwise loading - that is, whether or not the trailing vortices will combine into two or more rolled-up vortices - may not be known (ref. 13). If knowledge of the trailing-vortex behavior is unknown, it is believed that a fair quantitative representation of the vortex-system velocity gradient can still be made, for use in determining the range of airplane normal load factors, by employing the equations presented herein.

Load Factors

Elevator-fixed penetrations.- The normal-load-factor calculations, assuming rigid penetrating airplanes, include the load factors associated with the dynamic response of the airplanes to the vortex impulses. The assumption of a rigid structure for airplane P_A appears reasonable (ref. 14) for these calculations. However, if a penetrating airplane has a relatively flexible wing (such as, possibly, airplane P_B) the rigid-body treatment of the problem may not be adequate. Results of reference 15 show that the wing-root bending moments and fuselage center-line load factors of an elastic-body system can be 25 percent greater than for a rigid-body system subjected to like flight conditions. The increases are attributed to a dynamic-overshoot effect as the airplane penetrates a velocity gradient. A rule of thumb is given in reference 15 for deciding whether or not the airplane, when encountering a sine-shaped gust, may be treated as a rigid body. The rule states that "as long as the period ratio, the time to penetrate the gust to the point of maximum gust velocity divided by one-fourth the natural period of the fundamental wing bending mode, is of the order of 5 or greater, the airplane may be treated as a rigid body."

The normal load factors calculated for three penetrating-airplane velocities indicate two expected trends (fig. 7(a)). One trend is that peak load factors for a given airplane occur over corresponding shorter periods of time as the velocity of the penetrating airplane increases. The other trend is that the peak load factors show an increase in magnitude with corresponding increases of airplane velocity.

The load factors for the three center-of-gravity locations, illustrating the effect of airplane static stability, show that the peak values of load factor vary little with center-of-gravity location (fig. 7(b)). There are some differences in load factor between the peak values; however, the differences are of relatively small magnitude.

The calculated load factors for different levels of penetration indicate that as the airplane becomes more distant from the line of vortex centers the peak load factors rapidly diminish in magnitude, as would be expected (fig. 7(c)). Along penetration paths 25 feet above

or below the line of vortex centers the peak load factors from the 1 g steady flight datum are less than one-half the peak values calculated for the path coinciding with the line of vortex centers.

When the penetrating airplane enters the vortex system at angles to the line of vortex centers, and through the center of the core first approached, the peak maximum and minimum load factors experienced initially are approximately the same for entry angles to $\pm 45^{\circ}$, the extent of the investigation. As the airplane progresses along the penetration path the load factors then are seen to approach the steady-state or 1 g value with increasing rapidity as the penetrating angle increases (fig. 7(d)). The load factors approach the steady-state value rapidly after the initial peak values since the influence of the farthest vortex is small for angles of $\pm 15^{\circ}$ and $\pm 45^{\circ}$.

A comparison of the calculated load factors on the penetrating airplanes, traversing with elevator fixed the vortices of the three heavy transport airplanes (figs. 8 and 9), indicates that the design limit and ultimate load factors can be, in some cases, exceeded. The design ultimate load factors are exceeded on airplane P_A when traversing the wakes of airplanes G_B and G_C and on airplane P_B when traversing the wake of airplane G_C. The design limit load factor is exceeded on airplane P_B when traversing the wake of airplane G_B. The design load factors are not exceeded on either penetrating airplane when traversing the wake of airplane G_A. The peak load factors on airplane P_A are considerably greater than those on airplane P_B for comparable conditions because airplane P_A is much lighter than airplane P_B. However, the ratios of the incremental peak load factors (from the 1 g datum) to the respective design ultimate load factors of the penetrating airplanes for comparable conditions are approximately the same.

Estimated elevator motion.- The preceding discussion has been concerned with the penetrating airplanes traversing the vortex system with elevator fixed. Also investigated was the effect of an elevator control motion which might be made by a pilot in an effort to attenuate the normal load factors imposed by the vortices. As indicated in figure 10, the load factor n in this example exceeds both the design limit and the design ultimate load factors, whereas the design load factors were not exceeded when the same vortex system was traversed with elevator fixed.

Of course an elevator motion could either aggravate or alleviate the normal load factor on the airplane traversing the vortices, depending upon the phasing of the elevator deflection with the load factors imposed by the vortices. However, since the trailing vortices are normally invisible and an encounter unexpected, a deflection of the elevators

would in all probability, because of inherent pilot and control-system lag, cause greater peak load factors than if the elevators were held fixed.

Elevator Deflection Requirement

It is also of interest to determine the elevator deflection necessary to maintain 1 g flight for the penetrating airplane while traversing the vortices. As an example (case 16) the incremental elevator deflection required to maintain 1 g flight was calculated for airplane P_A. The calculations were made for case 16 primarily because the relatively small magnitude and low rate of change with time of airplane load factor for this case would require comparatively small incremental elevator deflections and deflection rates. The low rate of change of load factor also permitted adequate solutions of $\dot{n}$ and $\ddot{n}$ (first and second numerical differentiations of n), which were needed to solve for the elevator deflections.

As shown in figure 11, even if the required elevator motion could be anticipated by the pilot, the maximum deflection required to maintain 1 g flight for the example case is not within the capabilities of the control system.

Vertical Displacement

The vertical displacements of airplane P_A from the penetration path prescribed for cases 1 to 3 range from approximately 4 feet above the line of vortex centers to 8 feet below (fig. 12). Specifically, the displacements for case 2, for example, range from about 3 feet above to 8 feet below the line of vortex centers. From inspection of figure 7(c), which presents n for several values of h at the velocity of case 2, the effects of displacements of 3 feet or less in the region of the vortex cores would be expected to have little effect on the normal load factor. The 8-foot displacement which occurs well after the penetrating airplane passes through the second core would have negligible effect on the load factor. Thus it was concluded that, for the cases investigated, the effects of the vertical displacements on the normal load factors did not warrant inclusion in the present calculations.

CONCLUSIONS

The systematic calculation of normal load factor utilized available theories and accounted for normal translational velocity, lag in lift, and dynamic response in pitch of light airplanes traversing vortex fields.

The results indicate that light normal-category and light transport-category airplanes traversing wakes of currently operational heavy transport airplanes can experience loading conditions that exceed the design limit and, in some cases, the design ultimate load factors.

Load factors calculated for the light airplanes traversing the wake of a proposed supersonic transport were shown to exceed the design ultimate load factors by a comparatively large amount. Hence, because of the design trend toward heavy supersonic transports with short wing spans, penetrating airplanes can be expected to encounter loads of increased severity in the future.

The results show that lighter airplanes can be expected to experience greater load factors than heavier airplanes when traversing a vortex system under similar conditions. The ratios of the maximum load factor (from level flight) to the design ultimate load factor were, however, about the same for the two penetrating airplanes used in this analysis. It was found, furthermore, that the load factors on the penetrating airplane increased with velocity, reached maximum values near the vortex cores, and were not affected appreciably by center-of-gravity location. It was shown that the penetrating airplane must pass either through or very close to the rather confined areas of vortex cores to experience load factors of severe magnitude.

The results also show that although load factors imposed by the vortices could be alleviated by elevator deflection the pilot would be required to anticipate exactly the phasing of elevator motion with impulses from the vortices. However, because of inherent pilot and control-system lag, the loading conditions would almost certainly be aggravated rather than alleviated by elevator deflection.

Langley Research Center,
National Aeronautics and Space Administration,
Langley Field, Va., March 13, 1961.

APPENDIX A

SYMBOLS

a_n	normal acceleration, ft/sec^2
A	wing aspect ratio, b^2/S
b	wing span, ft
b_t	horizontal-tail span, ft
$\bar{c}$	wing mean aerodynamic chord, ft
C_L	lift coefficient, nW/qS
$C_{L,t}$	horizontal-tail lift coefficient, $(L/qS)_t$
C_m	pitching-moment coefficient of airplane without horizontal tail, Mb/qS^2
$C_{m,t}$	pitching-moment coefficient of isolated horizontal-tail surface
d	distance between core centers of the rolled-up trailing wing-tip vortices, ft
D_1,D_2,D_3,D_4	distances, ft (fig. 13)
e	distance behind wing at which trailing wing-tip vortices become essentially rolled up, ft
F(t)	impressed moment forcing function, $M/-I$, 1/sec^2
g	acceleration due to gravity, 32.2 ft/sec^2
h	penetration-path height from line of vortex centers, ft
I	pitching moment of inertia of airplane, slug-ft^2
k_Y	radius of gyration about pitching axis, ft
K'	empirical constant denoting ratio of damping moment of complete airplane to damping moment of tail alone

$K_1, K_2, \ldots K_6$ constants occurring in equation (B21) (defined in table V)

L lift, lb

m airplane mass, slugs

M impressed airplane pitching moment about the center of gravity, ft-lb

M_w pitching moment attributed to circulatory flow of vortices, ft-lb (defined by eq. (B19))

M_δ pitching moment attributed to elevator deflection, ft-lb (defined by eq. (B17))

n airplane normal load factor, a_n/g

n_1 load factor for trimmed steady flight ($n_1 = 1$)

n_r load factor due to airplane response

n_l load factor due to circulatory flow of vortices

q dynamic pressure, lb/sq ft

r radial distance from center of vortex core, ft

r_c radius of vortex core, ft

S wing area, sq ft

S_t horizontal-tail area, sq ft

t time after airplane entry into vortex field, sec

t_1, t_2, t_3, t_4 times at which the airplane enters and departs the vortex cores, sec (defined by eqs. (B8) and (B9))

V velocity of airplane, ft/sec

V_v normal translational velocity of airplane, ft/sec

w resultant velocity of vortices perpendicular to penetration path, ft/sec

w_c tangential velocity of circulatory flow inside the vortex core, ft/sec

w_d	downward velocity of rolled-up vortices, ft/sec
w_v	tangential velocity of circulatory flow in vortex outside the core, ft/sec
W	airplane weight, lb
x	distance along the penetration path where w is approximately 2 ft/sec, ft (fig. 13)
x_t	length from center of gravity of airplane to aerodynamic center of horizontal tail (positive when tail is rearward of center of gravity), ft
α	airplane angle of attack, radians
α_t	horizontal-tail angle of attack, radians
α_e	effective induced angle of attack, radians
α_l	α_w modified for lag-in-lift effects, radians
α_r	induced angle of attack due to airplane response, radians
α_v	induced angle of attack due to normal translational velocity of airplane, radians
α_w	induced angle of attack due to resultant velocity w of vortices, radians
γ	angle of penetration path with respect to line of vortex centers, deg
$\Delta\delta$	incremental elevator angle, radians
ϵ	downwash angle, $\frac{d\epsilon}{d\alpha}\alpha$, radians
η_t	tail efficiency factor, q_t/q
$\theta_1,\theta_2,\theta_3$	angles, deg (fig. 13)
θ_e	effective airplane pitch angle due to vortex circulatory flow, radians
ρ	mass density of air, slugs/cu ft

The notations $\dot{\alpha}$, $\dot{\theta}$, $\dot{n}$, $\ddot{n}$, and $\ddot{\alpha}$ denote first and second derivatives of variables with respect to time.

Subscripts:

g	generating airplane
p	penetrating airplane
t	horizontal tail

APPENDIX B

DETAILS OF METHODS USED

To formulate the methods used in this paper, well-known theoretical descriptions of wing-tip trailing vortices, as developed by a generating airplane, are first resolved to convenient form. The angles of attack on the penetrating airplane induced by the vortex flow were then determined and used to calculate the normal load factors.

Trailing Vortices

The transport airplane generating the vortices was assumed to have elliptical spanwise wing loading. In accordance with the following expressions from theory (ref. 12), each wing-tip trailing vortex was essentially rolled up at a distance e behind the wing, where

$$e = 0.280 \frac{A_g}{C_L} b_g \tag{B1}$$

and had at the initial rolled-up condition a strength (tangential velocity gradient of the circulatory flow) w_v such that

$$w_v = \left(\frac{2L}{\pi^2 b \rho r V}\right)_g \qquad (r \geqq r_c) \tag{B2}$$

The tangential velocity of circulatory flow within the core of each vortex ($r \leqq r_c$) for the initial rolled-up condition was considered to vary linearly from a maximum at the periphery ($r = r_c$) to zero at the core center ($r = 0$) as

$$w_c = \left(\frac{2L}{\pi^2 b \rho r_c V}\right)_g \frac{r}{r_c} \tag{B3}$$

The core radius is defined by the theory as

$$r_c = 0.155\left(\frac{b}{2}\right)_g \tag{B4}$$

and the distance between core centers of the vortices is given by

$$d = \frac{\pi}{4} b_g \tag{B5}$$

The vortex cores have a downward velocity with respect to the flight path as calculated from the relation

$$w_d = \frac{-4}{\pi^2} V_g \left(\frac{C_L}{\pi A}\right)_g \tag{B6}$$

A method was set up to evaluate the resultant velocities, contributed by the circulatory flow of the two vortex fields, perpendicular to the penetration paths. The resultant velocities at given times along the penetration paths parallel to the line of vortex centers outside the vortex cores ($h \geqq r_c$) can be expressed by

$$w = \left(\frac{2L}{\pi^2 b \rho V}\right)_g \left(\frac{\cos^2\theta_1}{D_1} - \frac{\cos^2\theta_2}{D_2}\right) \tag{B7}$$

where

$$D_1 = x - V_p t$$

$$D_2 = D_1 + d$$

$$\theta_1 = \tan^{-1} \frac{h}{D_1}$$

$$\theta_2 = \tan^{-1} \frac{h}{D_2}$$

as shown in figure 13(a). Also for the cases where the penetration paths coincide with the line of vortex centers ($h = 0$) the resultant velocities were calculated with equation (B7) except those within the cores. The resultant velocities within the cores were defined by the straight line joining the resultant velocities, calculated with equation (B7), at the times the penetrating airplane entered and departed the cores. The times the first core was entered and departed are given, respectively, as

$$\left.\begin{aligned} t_1 &= \frac{x - r_c}{V_p} \\ \text{and} \quad t_2 &= \frac{x + r_c}{V_p} \end{aligned}\right\} \tag{B8}$$

and for the second core the times are

$$\left.\begin{aligned} t_3 &= \frac{x + d - r_c}{V_p} \\ \text{and} \\ t_4 &= \frac{x + d + r_c}{V_p} \end{aligned}\right\} \tag{B9}$$

The resultant velocities perpendicular to penetration paths at angles to the line of vortex centers about the vortex center first approached by the penetrating airplane are, except within the vortex core,

$$w = \left(\frac{2L}{\pi^2 b \rho V}\right)_g \left(\frac{1}{D_1} - \frac{\cos^2 \theta_3}{D_3}\right) \tag{B10}$$

where:

$$D_1 = x - V_p t$$

$$D_3 = D_1 + d \cos \gamma$$

$$D_4 = d \sin \gamma$$

$$\theta_3 = \tan^{-1} \frac{D_4}{D_3}$$

as shown in figure 13(b). Resultant velocities in the region of the core entered were also defined by the straight line joining the resultant velocities, calculated with equation (B10), at the times the airplane entered and departed the vortex core. The equations used for expressing the times to enter and depart the core, t_1 and t_2, respectively, are the same as previously written (eqs. (B8)). In this analysis the penetration paths at angles to the reference line do not intercept the second core; hence t_3 and t_4 are not considered.

An example of the velocities w calculated with equations (B7), (B8), and (B9) for a penetration path coinciding with the line of vortex centers is given in figure 5 (case 2). In the subsequent calculations the velocities w are assumed to be of uniform strength across the wing span of the penetrating airplane at any instant of time during penetration of the vortices.

Equations (B7) and (B10), then, in conjunction with equations (B8) and (B9), are used in this report to describe the velocity gradients experienced by the penetrating airplane while traversing the trailing wing-tip vortices. The effect of the vortex-flow resultant velocity component parallel to the penetration paths on the load factors of the penetrating airplane was believed to be small and was therefore not included in the calculations. Also, the interaction between the vortices of the generating and penetrating airplanes was considered negligible.

Normal Load Factors

The normal load factor n on the penetrating airplane, while traversing the vortex fields, can be written as

$$n = n_1 + n_l + n_r \tag{B11}$$

and in coefficient form as

$$n = 1 + \left(\frac{dC_L}{d\alpha}\frac{qS}{W}\right)_p (\alpha_l + \alpha_r) \tag{B12}$$

To solve equation (B12) for n the incremental induced angles (α_l and α_r) must first be determined. The values of the other parameters in the equation are known for the penetrating airplane for which calculations are to be made.

Induced angle of attack α_l.- Two steps were taken to resolve the resultant vortex velocities w to the induced angle of attack α_l on the penetrating airplane (no pitch motion assumed) while traversing the trailing vortices. The first step taken evaluated

$$\alpha_w = \frac{w}{V_p} \tag{B13}$$

at times

$$t = \frac{x - D_1}{V_p} \tag{B14}$$

along the penetration path. Several examples of α_w are shown plotted in figure 14 for the different types of cases investigated. The

penetrating airplane was considered to enter the vortices at time $t = 0$ (arbitrarily selected at the point where $w \leqq 2$ ft/sec).

The second step evaluated α_l by making adjustments for the lag-in-lift effects (Küssner function) on the induced angle α_w. The procedure utilized was a superposition integral that approximated α_w by a series of step changes in angle of attack. The function of figure 15 (obtained from ref. 16) was applied to each unit change to account for the lag in lift. As illustrated in the figure, the angle-of-attack ratio α_l/α_w becomes unity at 8 wing-chord lengths of penetration into a step-velocity gradient. Examples of the induced angles of attack α_w and α_l on the penetrating airplane are shown in figure 16 for case 2. Also shown in the figure is the effective induced angle of attack α_e which will be derived later.

Induced angle of attack α_r.- The induced angle of attack α_r can be expressed in the differential equations for the longitudinal motion of an airplane, namely, equations summing the forces perpendicular to the relative wind and the pitching moments about the airplane center of gravity. Implicit in these equations are the assumptions of a rigid airplane, linear aerodynamic derivatives, and small changes in penetrating-airplane speed and penetration-path angles while traversing the vortices along a specified path. The equations are reducible (ref. 17) to the equivalent second-order differential equation of longitudinal motion

$$\ddot{\alpha}_r + K_1\dot{\alpha}_r + K_2\alpha_r + \frac{M}{-I} = 0 \tag{B15}$$

The term M is the impressed pitching moment on the airplane about the center of gravity; K_1 and K_2 are constants for any given set of flight conditions as defined in table V.

The impressed pitching moment on the penetrating airplane under the present considerations is the sum of the moments attributed to the circulatory flow of the vortices M_w and the moments due to elevator deflection M_δ. Hence

$$\frac{M}{-I} = (M_\delta + M_w)\frac{1}{-I} \tag{B16}$$

where

$$\frac{M_\delta}{-I} = -\Delta\delta \frac{\rho V^2}{2m}\left(-\frac{dC_{L,t}}{d\delta}\eta_t \frac{S_t x_t}{k_Y^2} + \frac{dC_{m,t}}{d\delta}\eta_t \frac{S_t^2}{b_t k_Y^2}\right.$$

$$\left. - \frac{dC_{L,t}}{d\alpha_t}\frac{dC_{L,t}}{d\delta}\frac{K'\eta_t^2}{\sqrt{\eta_t}}\frac{\rho}{2}\frac{x_t^2 S_t^2}{m k_Y^2}\right) \tag{B17}$$

which can be written in abbreviated form as

$$\frac{M_\delta}{-I} = -K_3\Delta\delta \tag{B18}$$

and

$$\frac{M_w}{-I} = \alpha_e \frac{-\rho V^2}{2m}\left[\frac{dC_m}{d\alpha}\frac{S^2}{bk_Y^2} - \frac{dC_{L,t}}{d\alpha_t}\eta_t \frac{S_t x_t}{k_Y^2}\left(1 - \frac{d\epsilon}{d\alpha}\right)\right]$$

$$+ \dot{\alpha}_e \frac{\rho V}{2m}\frac{dC_{L,t}}{d\alpha_t}\eta_t \frac{S_t x_t^2}{k_Y^2}\frac{d\epsilon}{d\alpha}$$

$$+ \dot{\theta}_e \frac{\rho V}{2m}\frac{dC_{L,t}}{d\alpha_t}\eta_t \frac{S_t x_t^2}{k_Y^2}\frac{K'}{\sqrt{\eta_t}} \tag{B19}$$

which in abbreviated form is written

$$\frac{M_w}{-I} = K_4\alpha_e + K_5\dot{\alpha}_e + K_6\dot{\theta}_e \tag{B20}$$

The positive directions of the sign conventions employed are shown in figure 17 and are the same as those used in reference 17. The K constants, as defined, are listed in table V.

Equation (B17) represents the moment about the airplane center of gravity attributed to an incremental elevator deflection from the trim position. In equation (B19) the term containing α_e represents the moment on the airplane caused by the effective angle of attack induced by the resultant velocity gradient of the vortices; the $\dot{\alpha}_e$ term was introduced to represent the moment due to lag in downwash at the tail;

and the $\dot{\theta}_e$ term represents the moment due to change in horizontal-tail angle of attack due to effective airplane pitch.

Equation (B15) can be rewritten, using equations (B16), (B18), and (B20) as

$$\ddot{\alpha}_r + K_1\dot{\alpha}_r + K_2\alpha_r = K_3\Delta\delta - (K_4\alpha_e + K_5\dot{\alpha}_e + K_6\dot{\theta}_e) \tag{B21}$$

which is the longitudinal equation for a damped pitching oscillation with the impressed moment forcing function

$$F(t) = K_3\Delta\delta - (K_4\alpha_e + K_5\dot{\alpha}_e + K_6\dot{\theta}_e) \tag{B22}$$

The longitudinal equation of motion (eq. (B21)) is solved for the induced angle of attack α_r, the response of the airplane about the penetration path while traversing the vortex system. To solve the equation, the evaluation of the K constants and time histories of the effective induced angle of attack α_e (no pitch motion), $\dot{\alpha}_e$, $\dot{\theta}_e$, and incremental elevator deflection $\Delta\delta$, if any, are required. The values of the K constants as determined for the flight conditions investigated are listed in table VI.

To resolve the previously determined induced angle α_l to the effective induced angle of attack α_e, an adjustment was made for the effect of the penetrating airplane's normal translational velocity on the induced angle of attack α_l (no pitch motion). The airplane's normal acceleration along the penetration path, attributed to the vortex velocity gradient, was calculated from

$$a_n = ng = \left(\frac{dC_L}{d\alpha}\frac{qS}{W}\right)_p \alpha_l g \tag{B23}$$

The normal translational velocity $V_{v,p}$ was then derived by integrating the acceleration a with respect to time, and the relation

$$\alpha_v = \frac{V_{v,p}}{V_p} \tag{B24}$$

was used to express the induced angle of attack on the penetrating airplane due to its normal translational velocity.

Hence, the effective induced angle of attack on the airplane while passing through the vortices with no pitch motion can be written

$$\alpha_e = \alpha_l + \alpha_v \tag{B25}$$

Time histories of the effective induced angle of attack α_e were determined for each case investigated. (See fig. 16 for a typical example.)

The methods used to evaluate the rates of change of effective angle of attack $\dot{\alpha}_e$ and effective pitching velocity $\dot{\theta}_e$ induced on the penetrating airplane by the angle of attack α_e are illustrated in figure 18. The values of $\dot{\alpha}_e$ and $\dot{\theta}_e$ were calculated from the expressions

$$\dot{\alpha}_e = \frac{\Delta\alpha_e V_p}{x_t} \tag{B26}$$

and

$$\dot{\theta}_e = \frac{-\Delta\alpha_e V_p}{x_t} \tag{B27}$$

Sufficient information is now available concerning the impressed moment forcing function $F(t)$ (eq. (B22)) to solve the longitudinal equation of motion (eq. (B21)) for the response α_r of the penetrating airplane while traversing the vortex system.

An example of a typical elevator-fixed impressed moment forcing function $F(t)$ calculated with equation (B22) for case 2 is shown in figure 19. The forcing-function time histories of cases 1 to 16 were similarly found, and the time histories were programed according to equation (B21) in an automatic digital computing machine. Initial conditions specified for equation (B21) were $\alpha_r = 0$, $\dot{\alpha}_r = 0$, and $\ddot{\alpha}_r = 0$ at $t = 0$. Solutions to equation (B21) for α_r were obtained at times selected along the penetration paths to represent adequately the airplane response. The unsteady-lift effects following a change in angle of attack (Wagner function) were relatively small and not included.

General solutions to equation (B21) are presented in chart form (fig. 20) for a range of airplane characteristics, and an example illustrating their use is given in appendix C.

Elevator Deflection Requirement

The incremental elevator deflection required for the attenuation of the load factor to 1 g flight through the vortex system is expressed by the relation given in reference 17 (with negative sign affixed) as

$$\Delta\delta = -\left(\frac{W/S}{K_3 \frac{dC_L}{d\alpha} q}\right)_p \left[\ddot{n} + K_1\dot{n} + K_2(n - 1)\right] \qquad (B28)$$

Sufficient information about the terms in equation (B28) is already available to solve for the incremental elevator deflection required of the penetrating airplane. The load factor n on the penetrating airplane traversing the vortices with elevator fixed is determined from equation (B11). The $\dot{n}$ and $\ddot{n}$ terms are determined by taking first and second derivatives of n.

Vertical Displacement

The vertical displacement of the airplane from the prescribed penetration path was obtained as a first approximation by integrating (numerically) twice with respect to time the normal acceleration a_n on the penetrating airplane where $a_n = (n - 1)g$.

APPENDIX C

EXAMPLE OF CHART APPLICATION

An example is given in this appendix to illustrate the generality of the charts in figure 20 for computing the normal load factor on the penetrating airplane P_A responding to an elevator deflection. The charts are solutions of equation (B21), in terms of airplane angle-of-attack response $K_2\alpha_r$, with unit forcing function $1(t)$ (that is, $F(t) = 0$ at $t < 0$ and $F(t) = 1$ at $t \geq 0$). The ranges of K_1 and K_2 represent values of airplane aerodynamic and geometric characteristics and flight conditions that are likely to exist.

The normal load factor n_r is defined as

$$n_r = \left(\frac{dC_L}{d\alpha}\frac{qS}{K_2W}\right)_p K_2\alpha_r \tag{C1}$$

where $K_2\alpha_r$ is defined in the relation

$$\ddot{\alpha}_r + K_1\dot{\alpha}_r + K_2\alpha_r = K_3\Delta\delta - (K_4\alpha_e + K_5\dot{\alpha}_e + K_6\dot{\theta}_e) \tag{C2}$$

Physical and aerodynamic characteristics of the airplane used in the example are given in table II and the flight conditions are the same as those of case 2. (See table III.)

The values of K_1 and K_2, as defined in table V, are also the same as those of case 2. (See table VI.) Interpolating in figure 20(e) ($K_1 \approx 6.0$ and $K_2 \approx 21.6$) gives the response $K_2\alpha_r$ of the airplane to a unit step function. This response is shown plotted in figure 21(a).

The next step is to evaluate the impressed moment forcing function $F(t)$ on the airplane from

$$F(t) = K_3\Delta\delta - (K_4\alpha_e + K_5\dot{\alpha}_e + K_6\dot{\theta}_e) \tag{C3}$$

The impressed moment used in this example is due only to an estimated incremental elevator deflection (shown plotted in fig. 10(a)); hence, $\alpha_e = 0$, $\dot{\alpha}_e = 0$, and $\dot{\theta}_e = 0$. From table VI, $K_3 = -32.52143$. The

time history of the derived impressed moment forcing function is plotted in figure 21(b).

Unit step functions are then superimposed on the plot of derived impressed moment forcing function so as to represent adequately the curve. At selected times the responses $K_2\alpha_r$ of each unit step are algebraically summed and the sums are each multiplied by 0.5111, the value of $\left(\frac{dC_L}{d\alpha}\frac{qS}{K_2W}\right)_p$ for the example, to obtain the load factor on the airplane n_r due to the impressed moment forcing function.

A comparison is made in figure 21(c) between the airplane normal load factors n_r calculated with the automatic computing machine and those determined by the superposition method using the charts. The agreement is considered to be good and illustrates that the charts are adequate for determining the response and load factors of an airplane with impressed moment. In a similar manner the incremental normal load factors could be calculated for other airplanes and/or flight conditions with the use of these charts.

REFERENCES

1. Anon.: Big Plane Turbulence Can Cause a Flight Hazard. Safety Suggestions No. 8, Beech Aircraft Corp., c.1952.

2. Crowley, H. G., and Chrisp, R. W.: Keep Your Distance. Safety Bull. No. 187-53, CAB.

3. Anon.: Accident Investigation Report - Lake Central Airlines, Inc. - Indianapolis, Indiana, August 21, 1952. File No. 1-0061, CAB, Apr. 10, 1953.

4. Anon.: Aircraft Accident Report - Piper Model PA-22, N 2945P, Near Dover, Delaware, September 23, 1958. File No. 2-0124, CAB, Oct. 10, 1959.

5. Kraft, Christopher C., Jr.: Flight Measurements of the Velocity Distribution and Persistence of the Trailing Vortices of an Airplane. NACA TN 3377, 1955.

6. Andrews, D. R.: A Flight Investigation of the Wake Behind a Meteor Aircraft, With Some Theoretical Analysis. C.P. No. 282, British A.R.C., 1956.

7. Kerr, T. H., and Dee, F.: A Flight Investigation Into the Persistence of Trailing Vortices Behind Large Aircraft. Tech. Note No. Aero. 2649, British R.A.E., Sept. 1959.

8. Anon.: Report of Project NR AVN 2656 - Effect of Wing-Tip Vortices and Sonic Shock on Army Aircraft in Flight. AD No. 134995 (U.S. Army Aviation Board, Fort Rucker, Ala.), Armed Services Tech. Information Agency, Doc. Service Center (Dayton, Ohio), May 1957.

9. Staff of the Langley Research Center: The Supersonic Transport - A Technical Summary. NASA TN D-423, 1960.

10. Anon.: Airplane Airworthiness - Normal, Utility, Acrobatic, and Restricted Purpose Categories. Pt. 03 of Civil Air Regulations, CAB, U.S. Dept. Commerce, Dec. 15, 1946.

11. Anon.: Airplane Airworthiness; Transport Categories. Pt. 4b of Civil Air Regulations, CAB, U.S. Dept. of Commerce, July 20, 1950.

12. Spreiter, John R., and Sacks, Alvin H.: The Rolling Up of the Trailing Vortex Sheet and Its Effect on the Downwash Behind Wings. Jour. Aero. Sci., vol. 18, no. 1, Jan. 1951, pp. 21-32, 72.

13. Bleviss, Zegmund O.: Theoretical Analysis of Light Plane Landing and Take-Off Accidents Due to Encountering the Wakes of Large Airplanes. Rep. No. SM-18647, Douglas Aircraft Co., Inc., Dec. 1954.

14. Pierce, Harold B.: Investigation of the Dynamic Response of Airplane Wings to Gusts. NACA TN 1320, 1947.

15. Kordes, Eldon E., and Houbolt, John C.: Evaluation of Gust Response Characteristics of Some Existing Aircraft With Wing Bending Flexibility Included. NACA TN 2897, 1953.

16. Jones, Robert T.: The Unsteady Lift of a Wing of Finite Aspect Ratio. NACA Rep. 681, 1940.

17. Pearson, Henry A., McGowan, William A., and Donegan, James J.: Horizontal Tail Loads in Maneuvering Flight. NACA Rep. 1007, 1951. (Supersedes NACA TN 2078.)

TABLE I

GENERATING-AIRPLANE CHARACTERISTICS

Characteristics	Airplane		
	G_A	G_B	G_C
Weight, lb	180,000	295,000	400,000
Wing span, ft	174.1	141.5	90.0
Wing area, sq ft	2,506	2,908	4,300
Wing aspect ratio	12.10	6.88	1.88
Velocity, ft/sec	253	322	420
Altitude, ft	1,000	1,000	1,000

TABLE II

PENETRATING-AIRPLANE CHARACTERISTICS

Geometric	Airplane P_A	Airplane P_B
Airplane weight, W, lb	2,000	35,000
Gross wing area, S, sq ft	147.5	754.0
Wing span, b, ft	29.3	95.2
Wing aspect ratio, A	5.82	12.00
Wing mean aerodynamic chord, $\bar{c}$, ft	5.25	8.45
Horizontal tail area, S_t, sq ft	27.2	172.0
Horizontal tail span, b_t, ft	9.54	31.65
Tail length, x_t, ft:		
Center of gravity, 20 percent $\bar{c}$	12.11	------
Center of gravity, 25 percent $\bar{c}$	11.85	------
Center of gravity, 30 percent $\bar{c}$	11.59	35.70
Radius of gyration, k_Y, ft	4.22	15.50
Elevator deflection, δ, radians:		
Maximum up	0.4188	------
Maximum down	0.2269	------
Aerodynamic		
Slope of airplane lift curve, $dC_L/d\alpha$, per radian	4.18	5.17
Slope of tail lift curve, $dC_{L,t}/d\alpha_t$, per radian	3.66	4.32
Downwash factor, $d\epsilon/d\alpha$	0.445	0.352
Tail efficiency factor, η_t	1.00	1.00
Empirical airplane damping factor, K'	1.10	1.10
Elevator effectiveness factor, $dC_{L,t}/d\delta$, per radian	2.93	1.73
Rate of change of tail moment with camber due to elevator angle, $dC_{m,t}/d\delta$, per radian	-0.57	-0.50
Rate of change of moment coefficient with angle of attack for airplane without tail, $dC_m/d\alpha$, per radian:		
Center of gravity, 20 percent $\bar{c}$	0.075	------
Center of gravity, 25 percent $\bar{c}$	0.284	------
Center of gravity, 30 percent $\bar{c}$	0.490	1.118

TABLE III

PENETRATING-AIRPLANE FLIGHT CONDITIONS

[Altitude, 1,000 feet; mass density of air, 0.002309 slug/cu ft]

Case	Penetrating airplane	V_p, ft/sec	γ, deg	h, ft	c.g. location, percent $\bar{c}$	$\Delta\delta$, radians	Generating airplane
1	P_A	117	0	0	25	0	G_A
2	P_A	176	0	0	25	0	G_A
3	P_A	205	0	0	25	0	G_A
4	P_A	176	0	0	30	0	G_A
5	P_A	176	0	0	20	0	G_A
6	P_A	176	0	±15	25	0	G_A
7	P_A	176	0	±25	25	0	G_A
8	P_A	205	±15	---	25	0	G_A
9	P_A	205	±45	---	25	0	G_A
10	P_A	205	0	0	25	0	G_B
11	P_A	205	0	0	25	0	G_C
12	P_B	338	0	0	30	0	G_A
13	P_B	338	0	0	30	0	G_B
14	P_B	338	0	0	30	0	G_C
15	P_A	176	0	0	25	See fig. 10(a)	G_A
16	P_A	117	0	±15	25	0	G_A

TABLE IV

GENERATING-AIRPLANE VORTEX PARAMETERS

Airplane	e, ft	r_c, ft	w_v at r_c, ft/sec	d, ft	x, ft	w_d, ft/sec
G_A	616	13.50	26.5	137.0	200	2.6
G_B	322	10.96	51.7	111.1	300	5.1
G_C	104	6.98	133.1	70.7	500	13.1

TABLE V

DEFINITION OF CONSTANTS OCCURRING IN THE LONGITUDINAL EQUATION OF MOTION

Constant	Definition
K_1	$\frac{\rho V}{2m}\left[\frac{dC_{L,t}}{d\alpha_t}\frac{S_t x_t^2}{k_Y^2}\eta_t\left(\frac{K'}{\sqrt{\eta_t}}+\frac{d\epsilon}{d\alpha}\right)+\frac{dC_L}{d\alpha}S\right]$
K_2	$-\frac{\rho V^2}{2m}\left\{\frac{dC_m}{d\alpha}\frac{S^2}{k_i^2 b}-\frac{dC_{L,t}}{d\alpha_t}\eta_t\frac{S_t x_t}{k_Y^2}\left[\left(1-\frac{d\epsilon}{d\alpha}\right)+\frac{dC_L}{d\alpha}\frac{K'}{\sqrt{\eta_t}}\frac{\rho}{2}\frac{Sx_t}{m}\right]\right\}$
K_3	$\frac{\rho V^2}{2m}\left(-\frac{dC_{L,t}}{d\delta}\eta_t\frac{S_t x_t}{k_Y^2}+\frac{dC_{m,t}}{d\delta}\eta_t\frac{S_t^2}{b_t k_Y^2}-\frac{dC_{L,t}}{d\alpha_t}\frac{dC_{L,t}}{d\delta}\frac{K'\eta_t^2}{\sqrt{\eta_t}}\frac{\rho}{2}\frac{x_t^2 S_t^2}{mk_Y^2}\right)$
K_4	$-\frac{\rho V^2}{2m}\left[\frac{dC_m}{d\alpha}\frac{S^2}{bk_Y^2}-\frac{dC_{L,t}}{d\alpha_t}\eta_t\frac{S_t x_t}{k_Y^2}\left(1-\frac{d\epsilon}{d\alpha}\right)\right]$
K_5	$\frac{\rho V}{2m}\left(\frac{dC_{L,t}}{d\alpha_t}\eta_t\frac{S_t x_t^2}{k_Y^2}\frac{d\epsilon}{d\alpha}\right)$
K_6	$\frac{\rho V}{2m}\left(\frac{dC_{L,t}}{d\alpha_t}\eta_t\frac{S_t x_t^2}{k_Y^2}\frac{K'}{\sqrt{\eta_t}}\right)$

TABLE VI

VALUES OF K CONSTANTS OCCURRING IN LONGITUDINAL EQUATIONS OF MOTION FOR THE VARIOUS CASES

Case	K_1	K_2	K_3	K_4	K_5	K_6
1	3.96273	9.52813	-14.37206	6.30771	0.75701	1.87150
2	5.96240	21.56047	-32.52143	14.27322	1.13902	2.81590
3	6.94393	29.25070	-44.12123	19.36422	1.32652	3.27945
4	5.79076	15.85335	-31.82337	8.88237	1.08958	2.69369
5	4.60787	27.34639	-33.22020	19.73585	1.18955	2.94082
6	5.96240	21.56047	-32.52143	14.27322	1.13902	2.81590
7	5.96240	21.56047	-32.52143	14.27322	1.13902	2.81590
8	6.94393	29.25070	-44.12123	19.36422	1.32652	3.27945
9	6.94393	29.25070	-44.12123	19.36422	1.32652	3.27945
10	6.94393	29.25070	-44.12123	19.36422	1.32652	3.27945
11	6.94393	29.25070	-44.12123	19.36422	1.32652	3.27945
12	3.45413	7.48648	-5.76739	5.30838	.49809	1.55654
13	3.45413	7.48648	-5.76739	5.30838	.49809	1.55654
14	3.45413	7.48648	-5.76739	5.30838	.49809	1.55654
15	5.96240	21.56047	-32.52143	14.27322	1.13902	2.81590
16	3.96273	9.52813	-14.37206	6.30771	.75701	1.87150

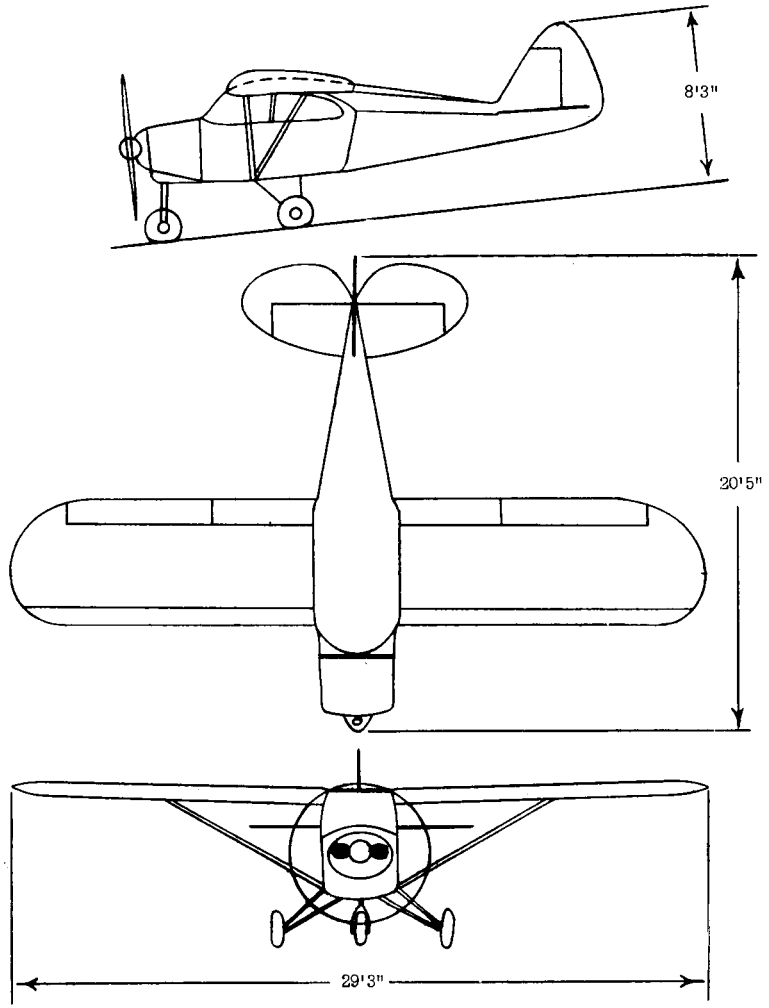

(a) Light normal-category airplane (airplane P_A).

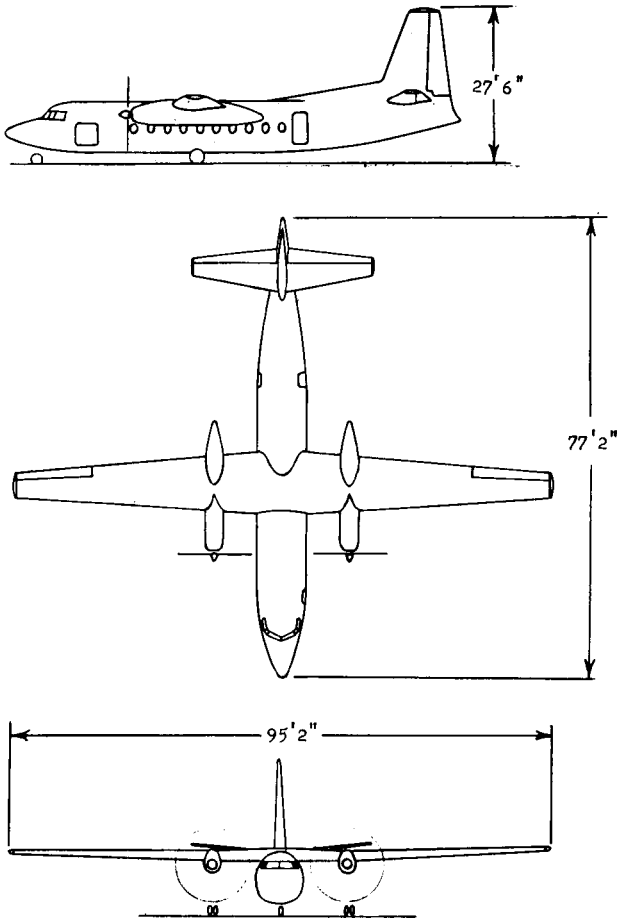

(b) Light transport-category airplane (airplane P_B).

Figure 1.- Penetrating-airplane configurations.

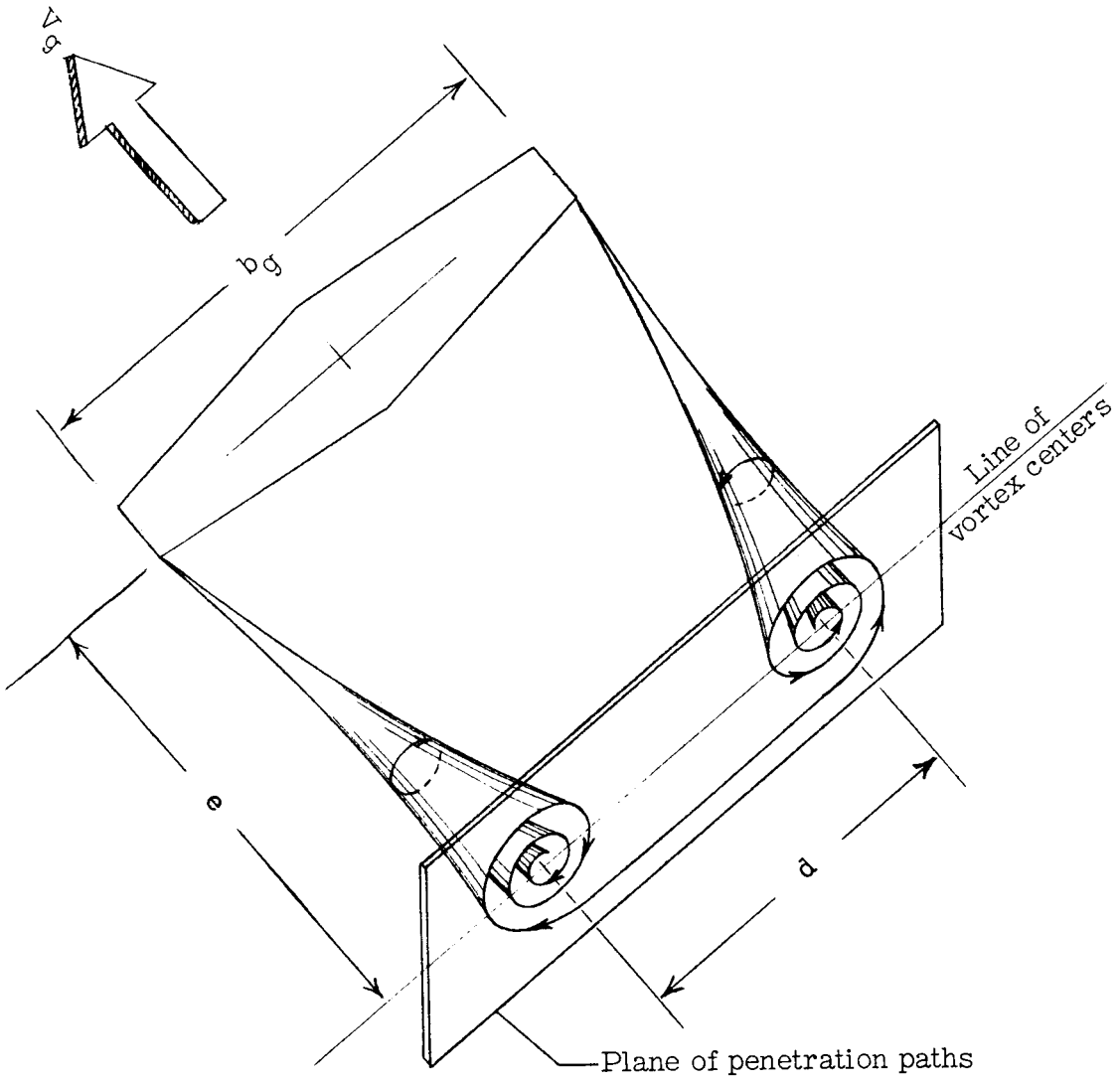

Figure 2.- Schematic sketch of wing-tip rolled-up trailing vortices shed by generating airplanes.

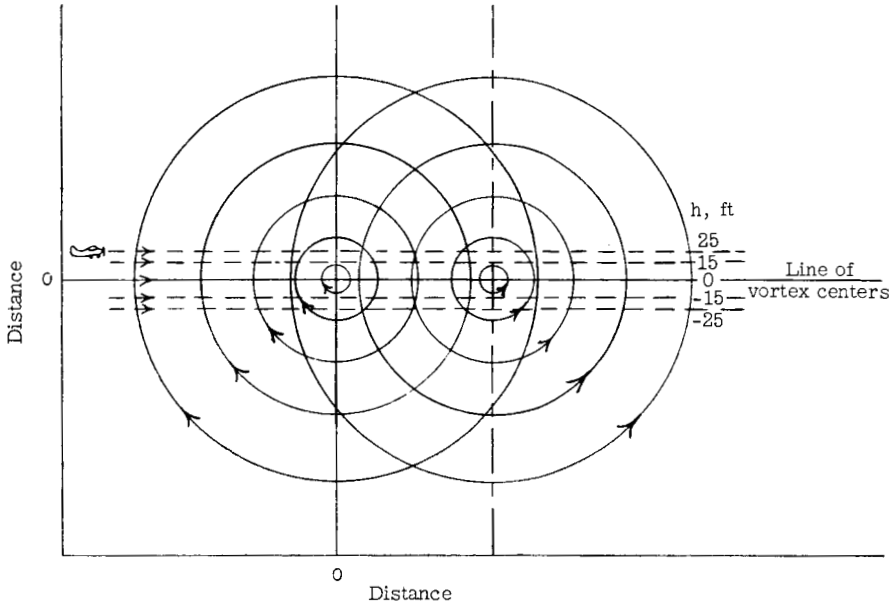

(a) Penetrating heights h.

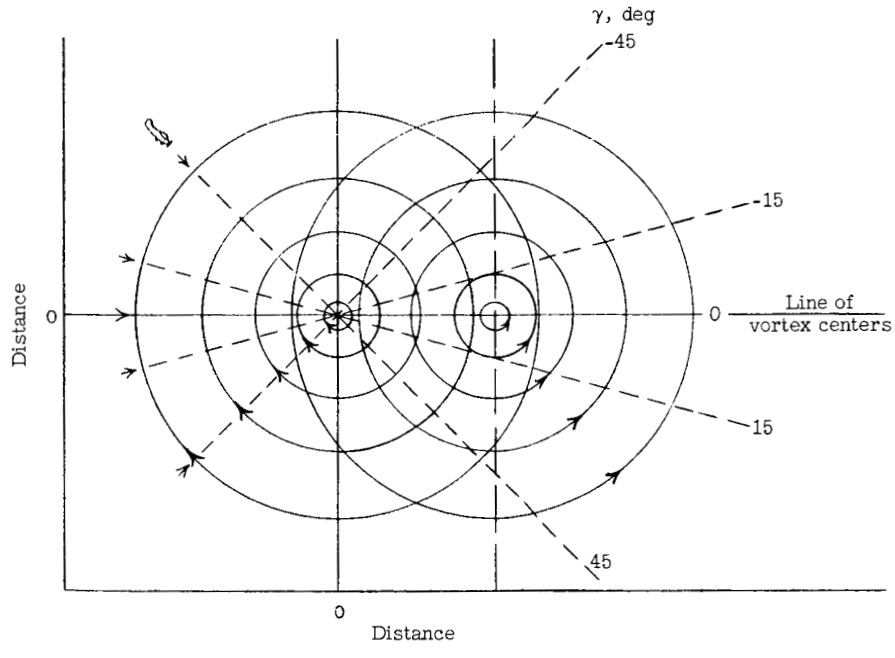

(b) Penetration angles γ.

Figure 3.- Schematic sketch of the selected penetration paths through the trailing vortices.

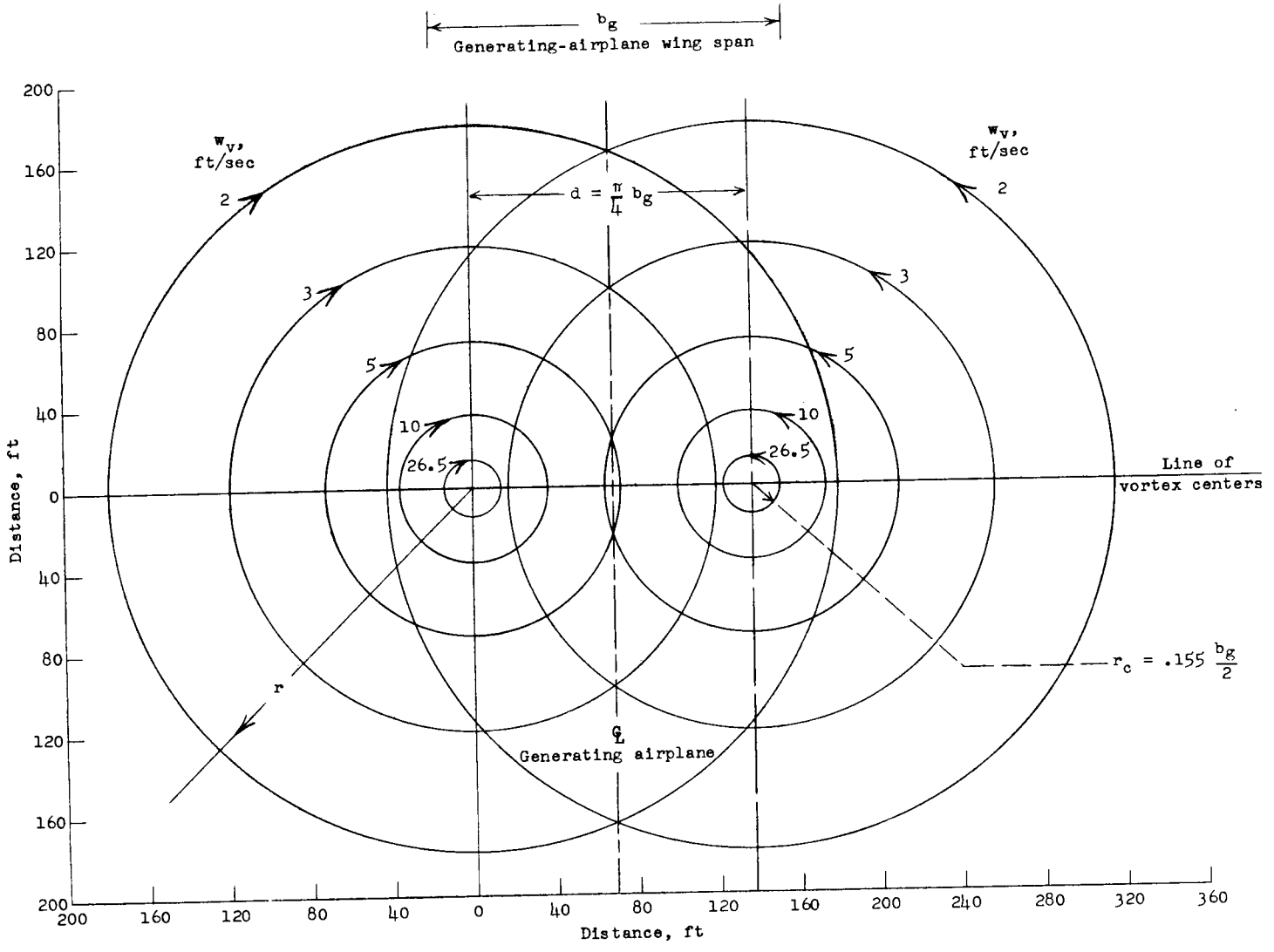

Figure 4.- Example of initial circulatory velocity w_v contours of rolled-up trailing vortices in the plane of penetration paths. Calculated for airplane G_A.

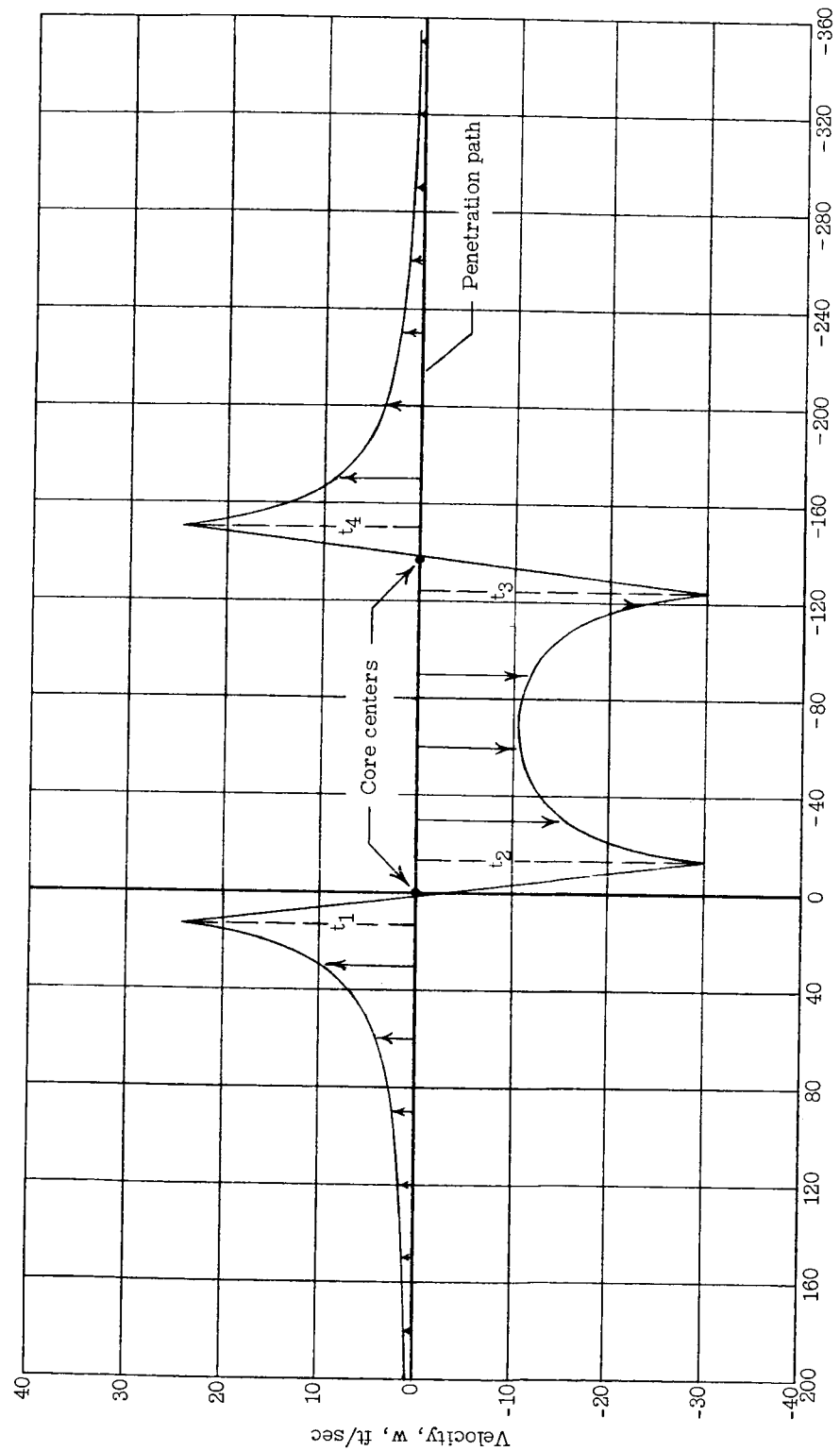

Figure 5.- Example of calculated velocity gradient perpendicular to penetration path. Case 2.

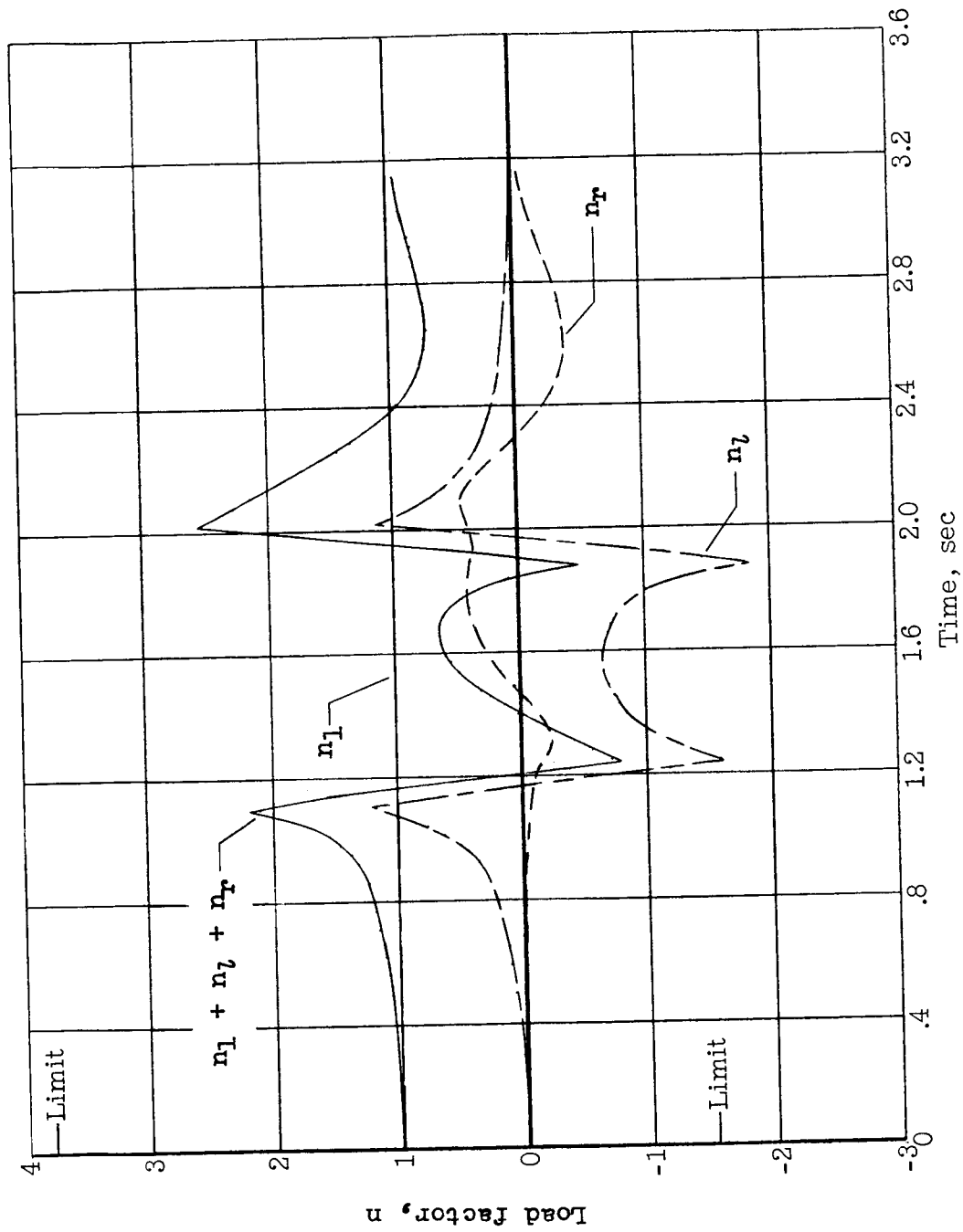

Figure 6.- Example of calculated load factors on penetrating airplane with elevator fixed traversing the wing-tip trailing vortices. Case 2.

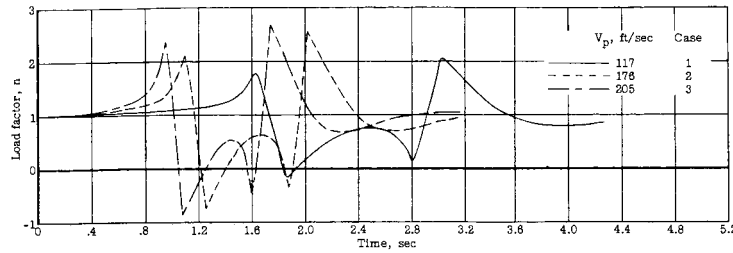

(a) Variation of penetration velocity.

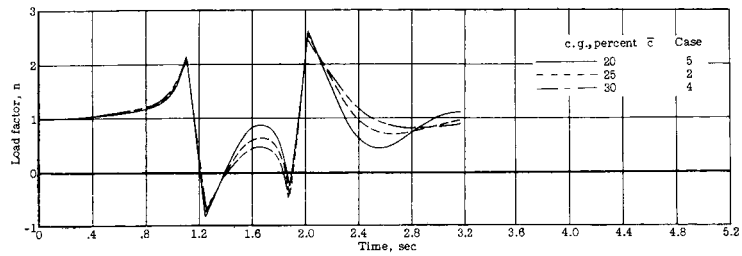

(b) Variation of center-of-gravity location.

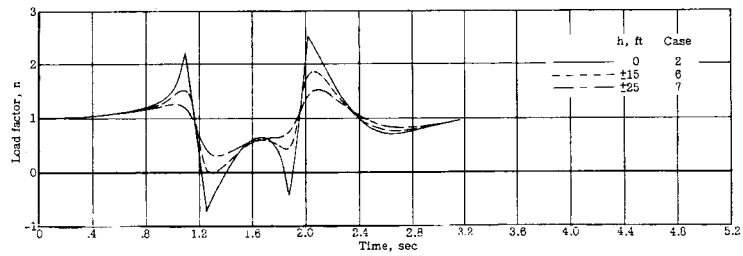

(c) Variation of penetration level.

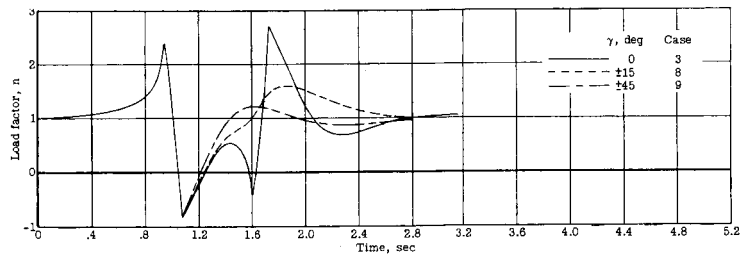

(d) Variation of penetration angle.

Figure 7.- The effects of several variables on the calculated load factors on airplane P_A with elevator fixed traversing the rolled-up trailing vortices of airplane G_A.

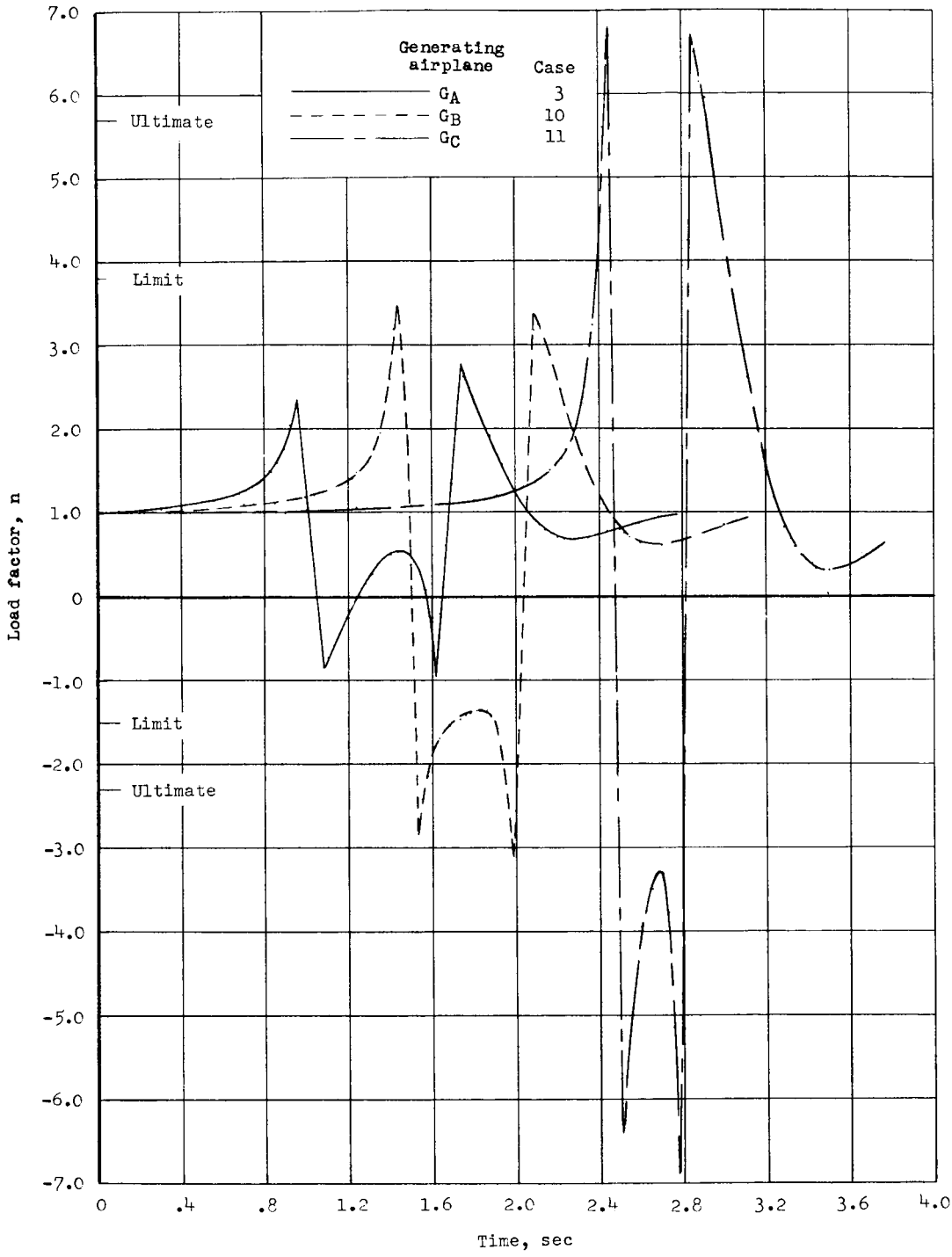

Figure 8.- Calculated load factors on airplane P_A with elevator fixed traversing the trailing vortices of airplanes G_A, G_B, and G_C.

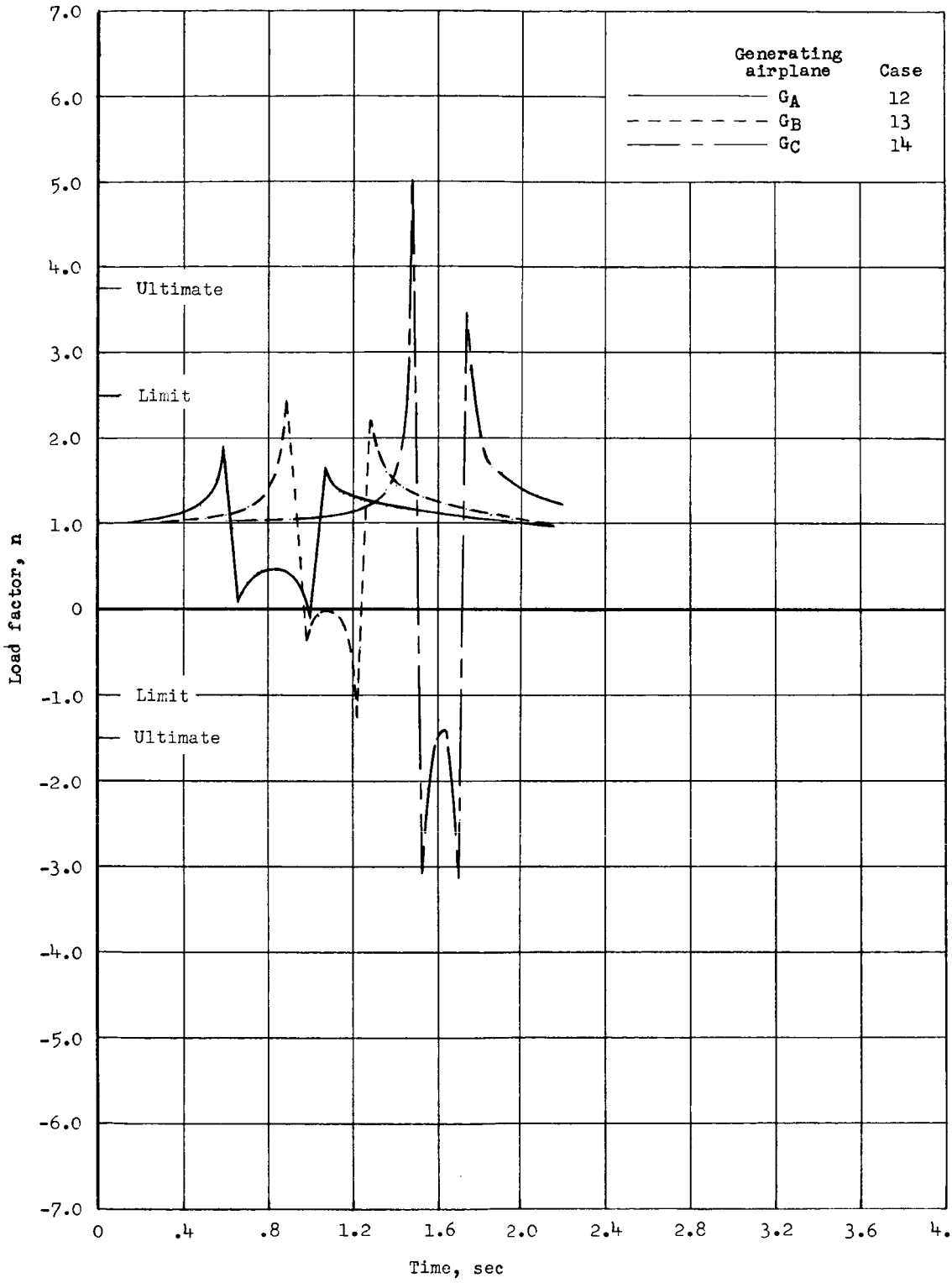

Figure 9.- Calculated load factors on airplane P_B with elevator fixed traversing the trailing vortices of airplanes G_A, G_B, and G_C.

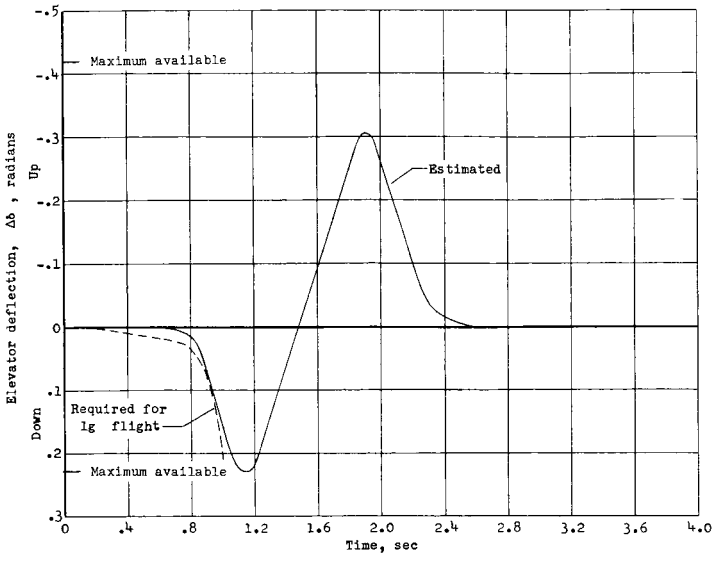

(a) Estimated elevator motion.

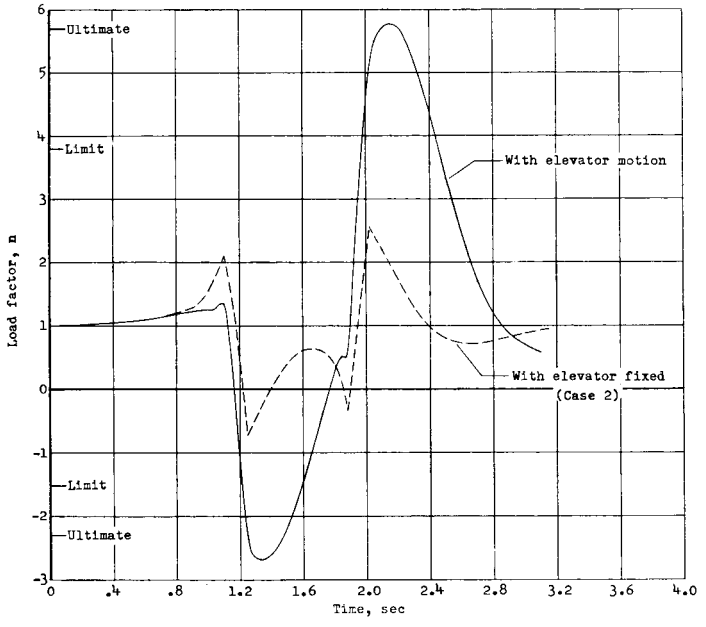

(b) Airplane load factor.

Figure 10.- Calculated load factors on airplane P_A with an estimated elevator motion traversing the trailing vortices of airplane G_A. Case 15.

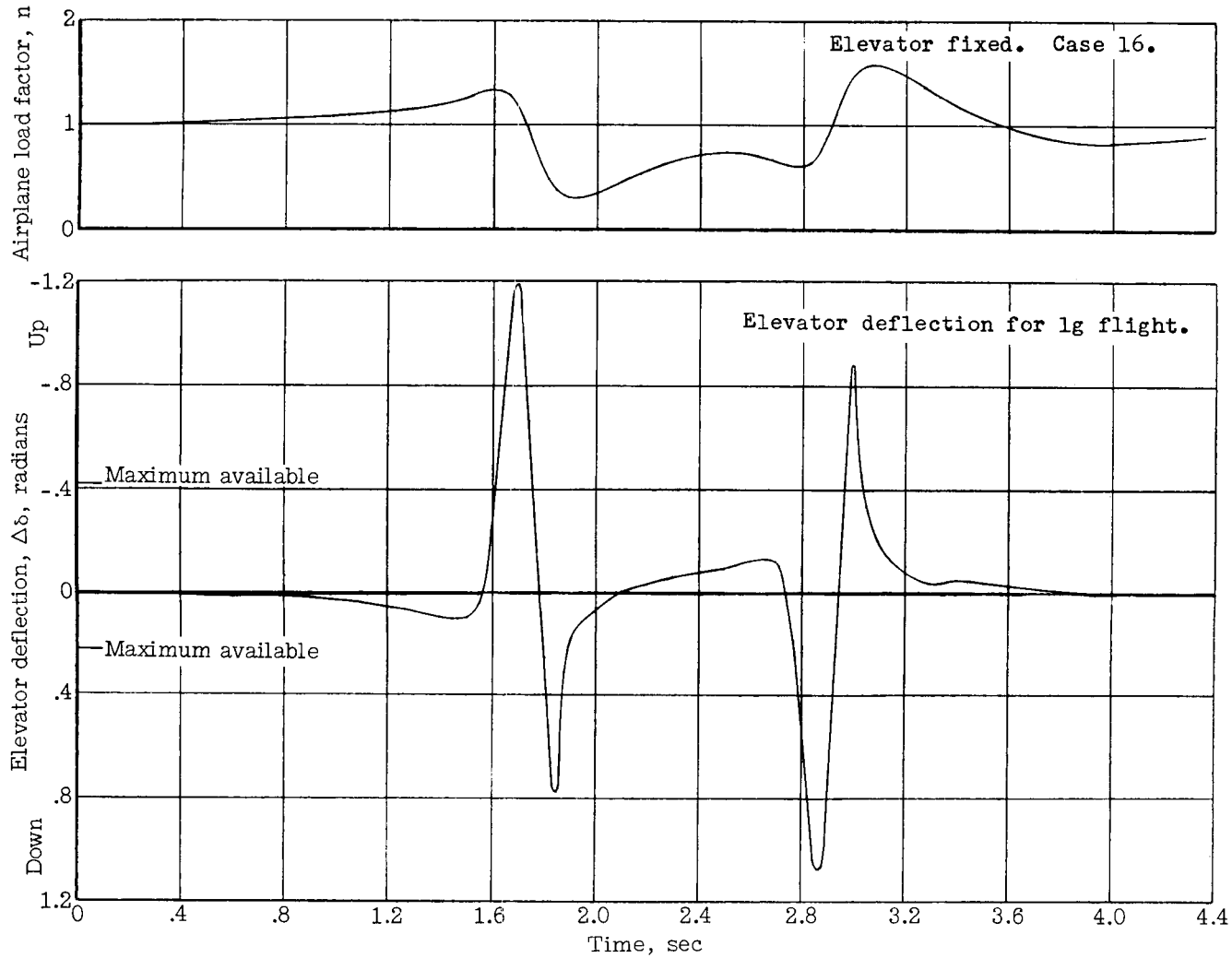

Figure 11.- Example of calculated elevator motion required for 1 g flight of airplane P_A through the vortices of airplane G_A.

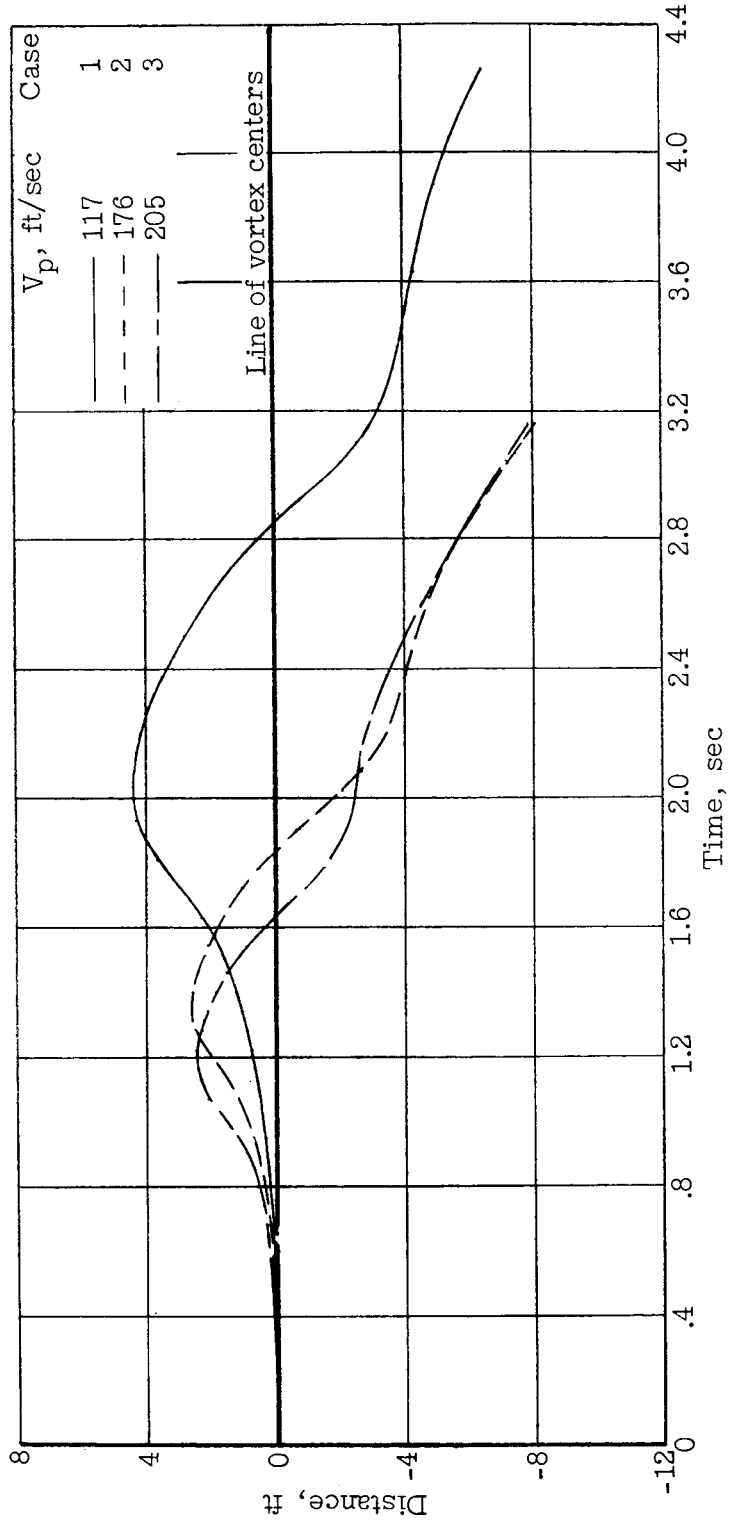

Figure 12.- Vertical displacement of airplane P_A with elevator fixed while traversing the trailing vortices of airplane G_A.

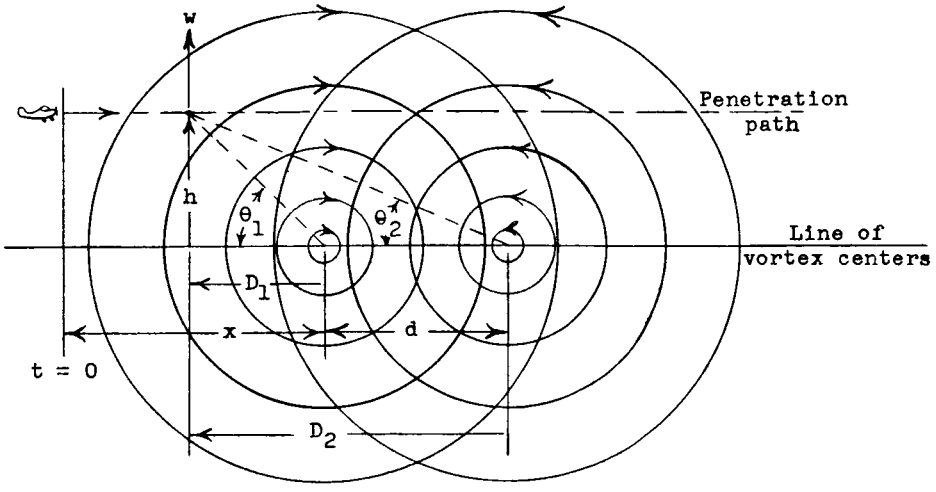

(a) Penetration paths parallel to the line of vortex centers at a distance h.

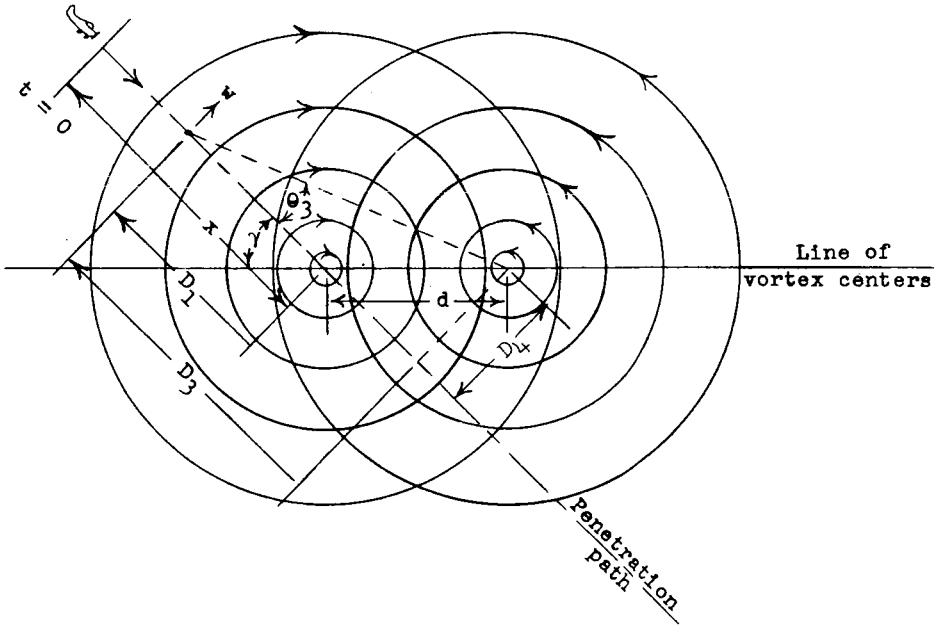

(b) Penetration paths at an angle γ with the line of vortex centers.

Figure 13.- Conventions used in calculating the resultant vortex velocities w perpendicular to the penetration paths. Positive directions of quantities shown.

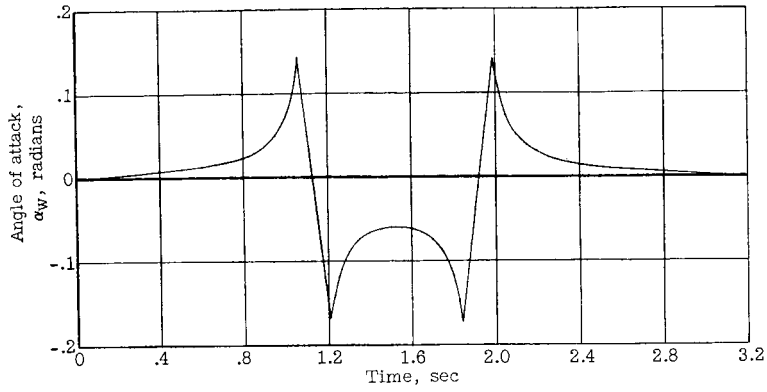

(a) Flight path on line of vortex centers.

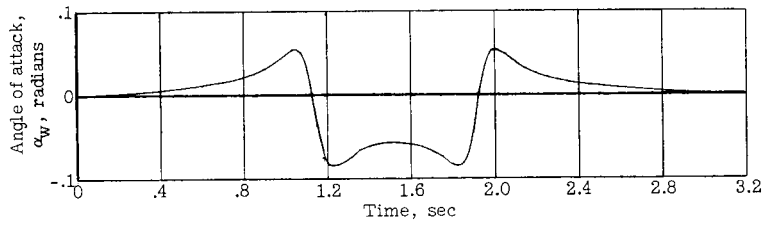

(b) Flight path at a distance parallel to the line of vortex centers. h = ±15 ft.

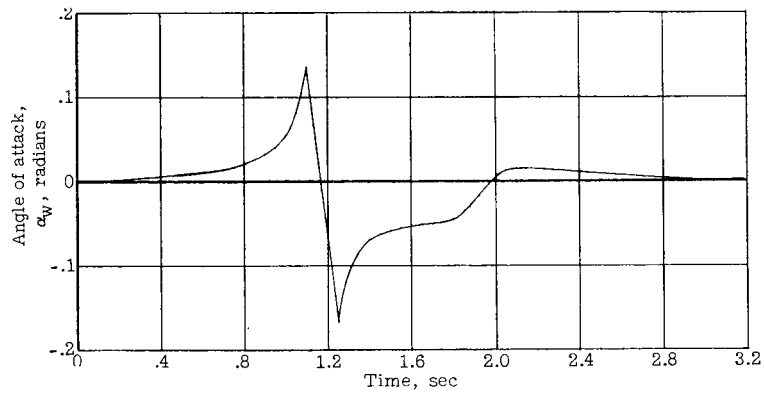

(c) Flight path at an angle to the line of vortex centers. $\gamma = \pm 15^{\circ}$.

igure 14.- Examples of angle of attack induced on penetrating airplane by the trailing vortices for the different types of cases investigated. V_p = 176 ft/sec.

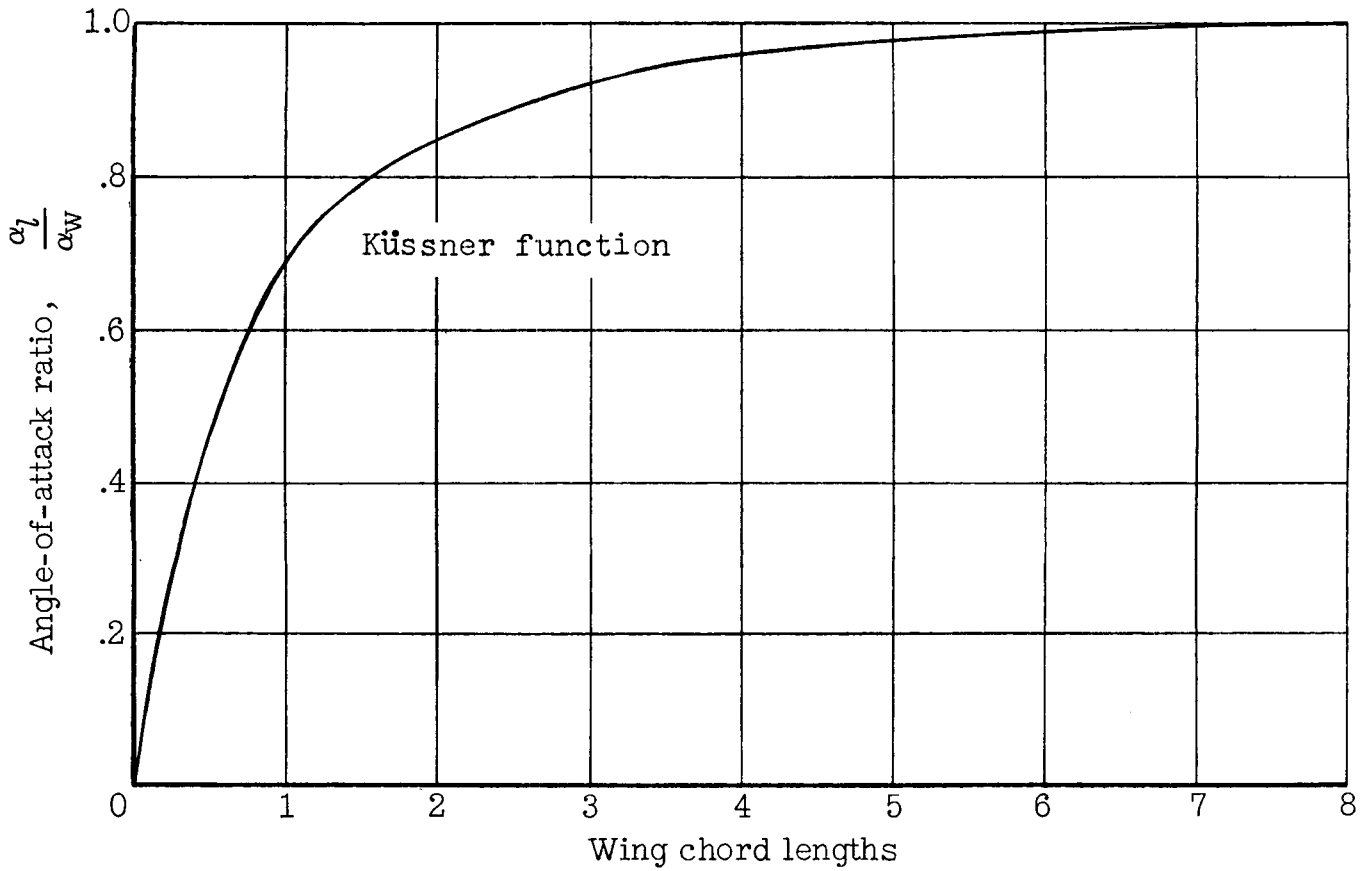

Figure 15.- Development of induced angle of attack on a wing penetrating a sharp-edge gust (lag in lift). A = 6. (From ref. 16.)

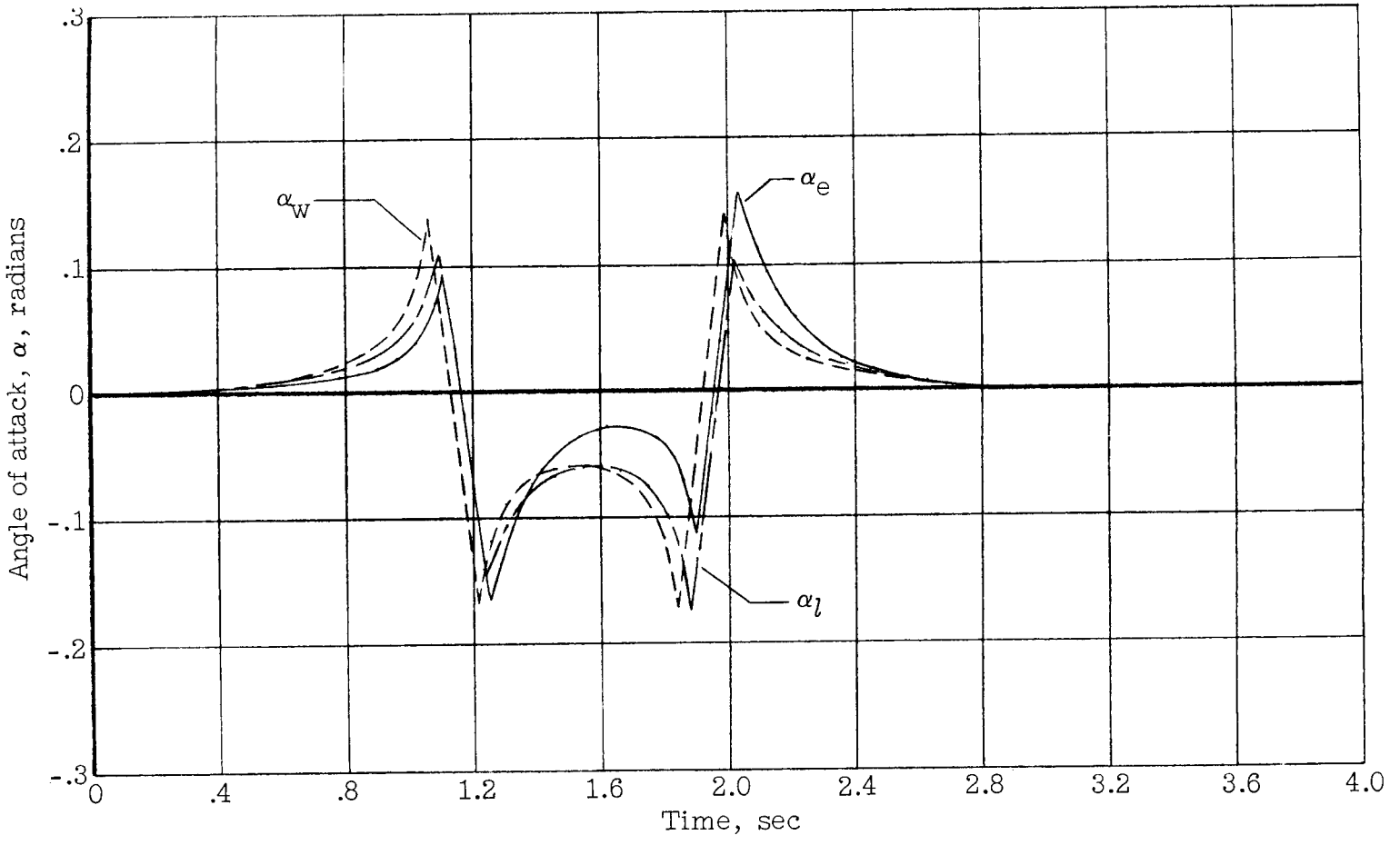

Figure 16.- An example of the effects of lag in lift and airplane normal translational velocity on the induced angle of attack on the penetrating airplane. $\alpha_v = \alpha_e - \alpha_l$; case 2.

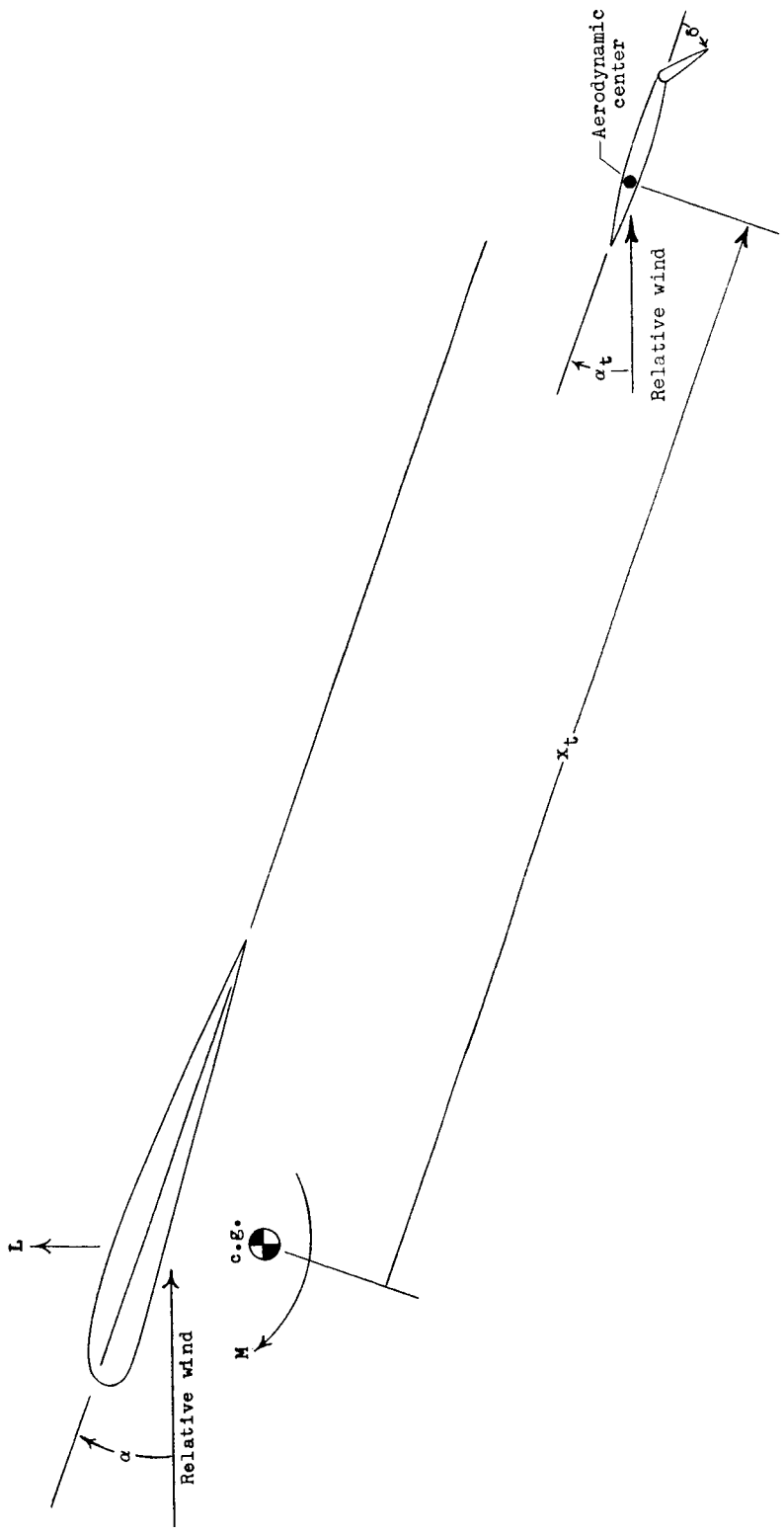

Figure 17.- Sign conventions employed. Positive directions shown.

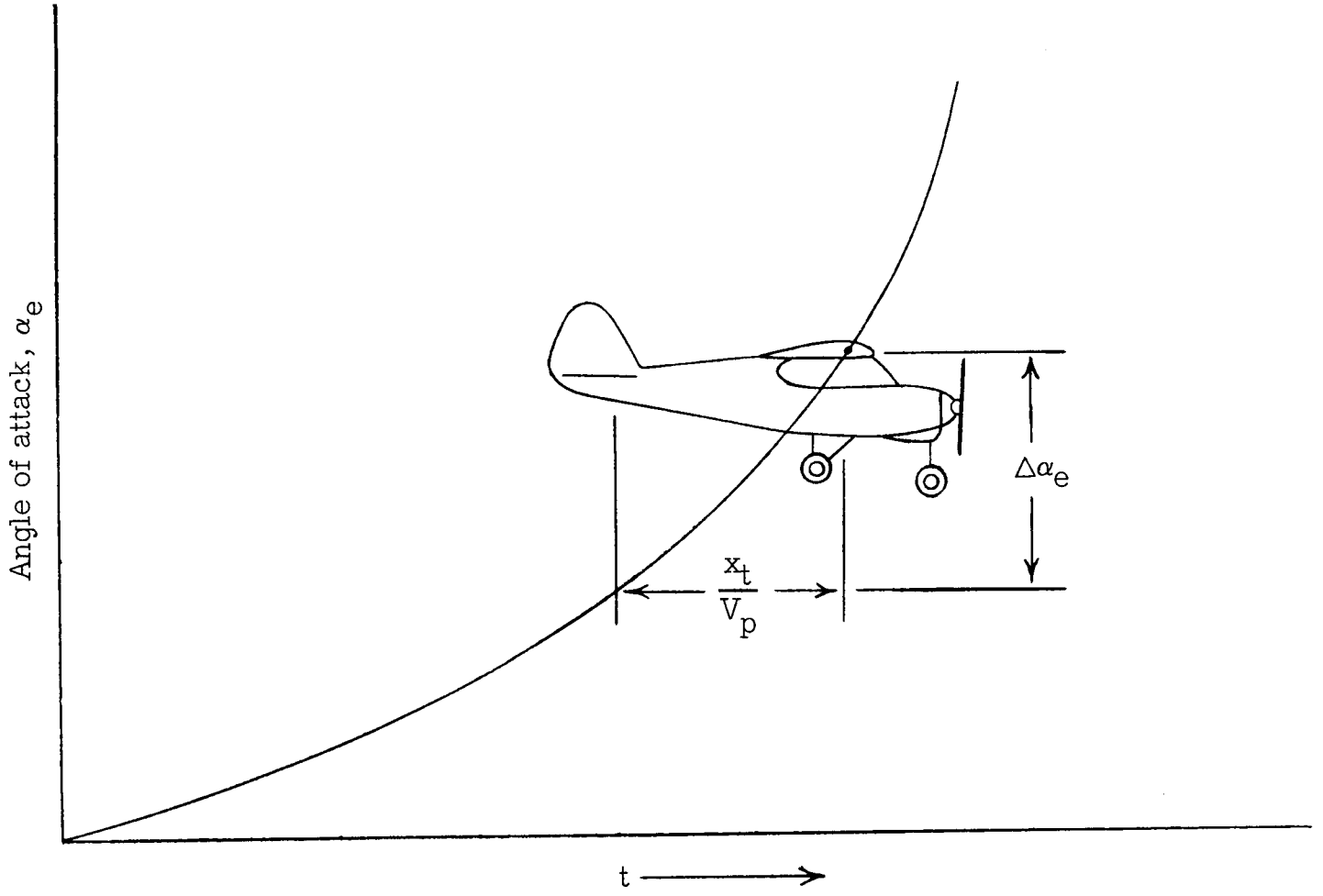

Figure 18.- Method used to determine the effective $\dot{\alpha}_e$ and $\dot{\theta}_e$ induced on the penetrating airplane by the vortex (no pitch motion). $\dot{\theta}_e = \frac{-\Delta\alpha_e V_p}{x_t}$; $\dot{\alpha}_e = \frac{\Delta\alpha_e V_p}{x_t}$.

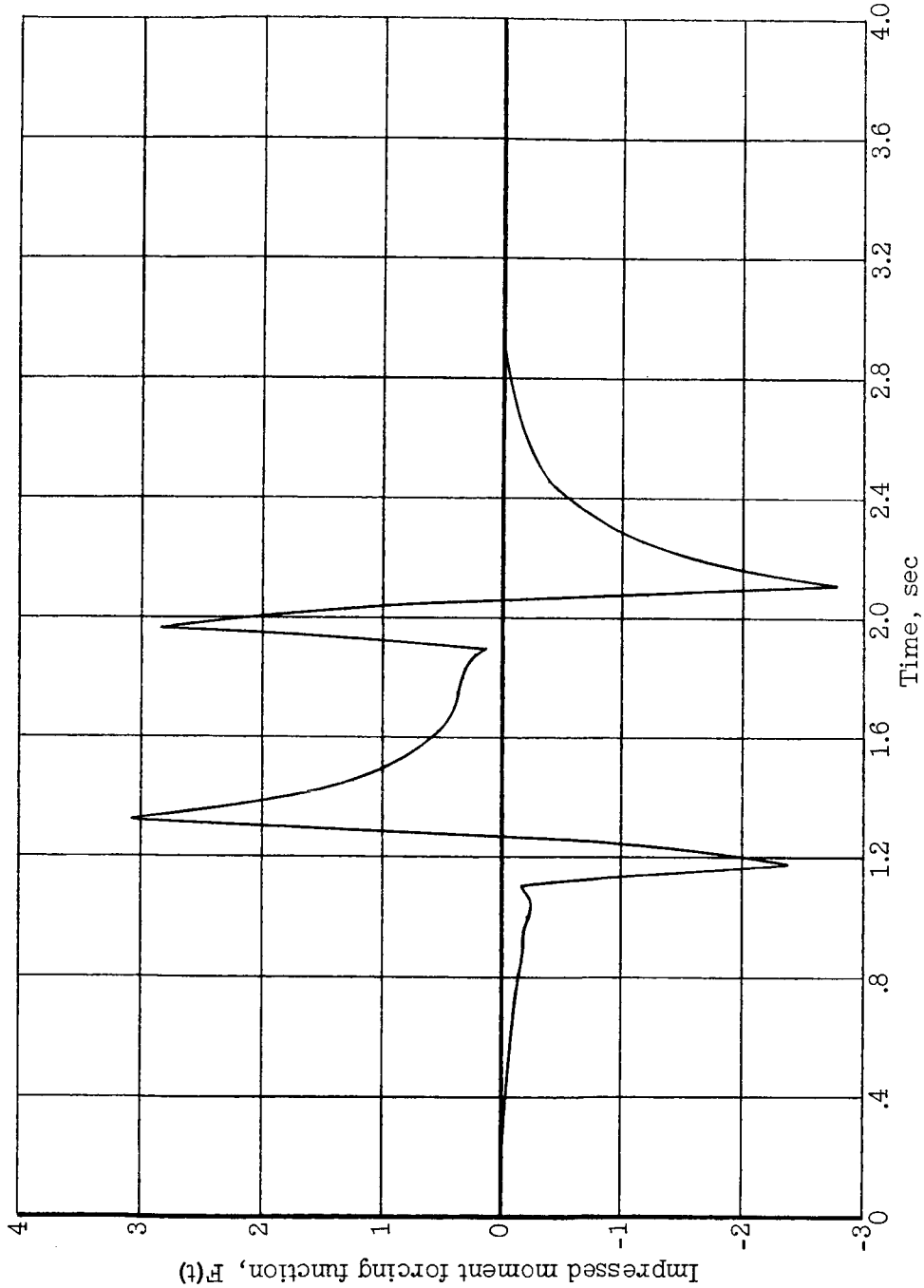

Figure 19.- Example of a typical elevator-fixed impressed moment forcing function F(t). Calculated for case 2; $\Delta\delta = 0$.

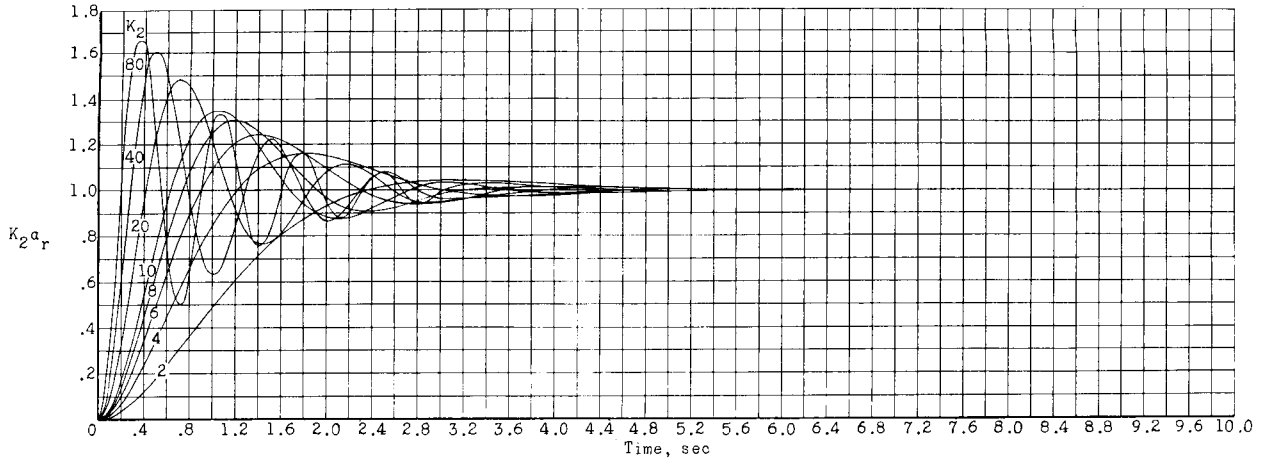

(a) $K_1 = 2.$

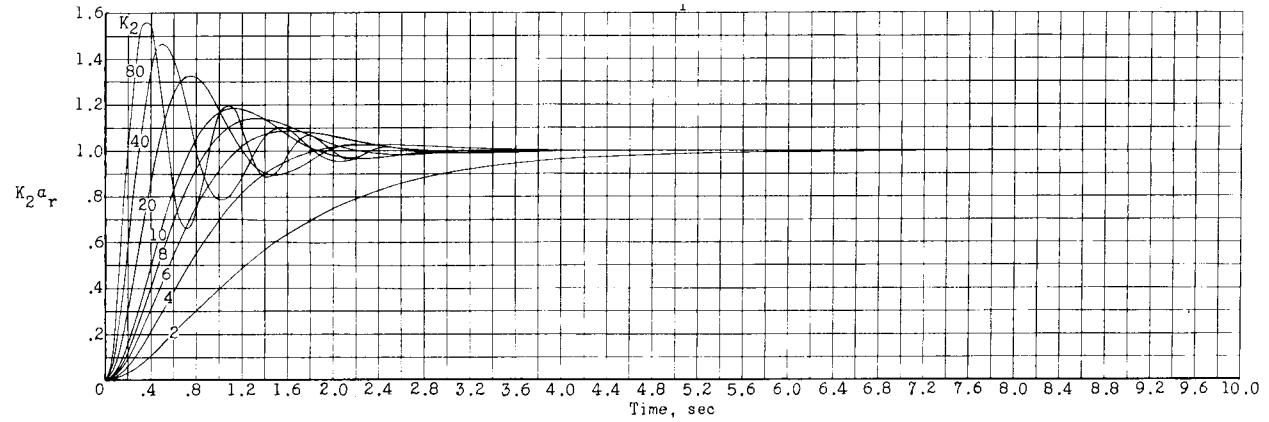

(b) $K_1 = 3.$

Figure 20.- Variations of $K_2 a_r$ with time for a unit step function $F(t) = 1(t)$ for series of K_1 and K_2 terms.

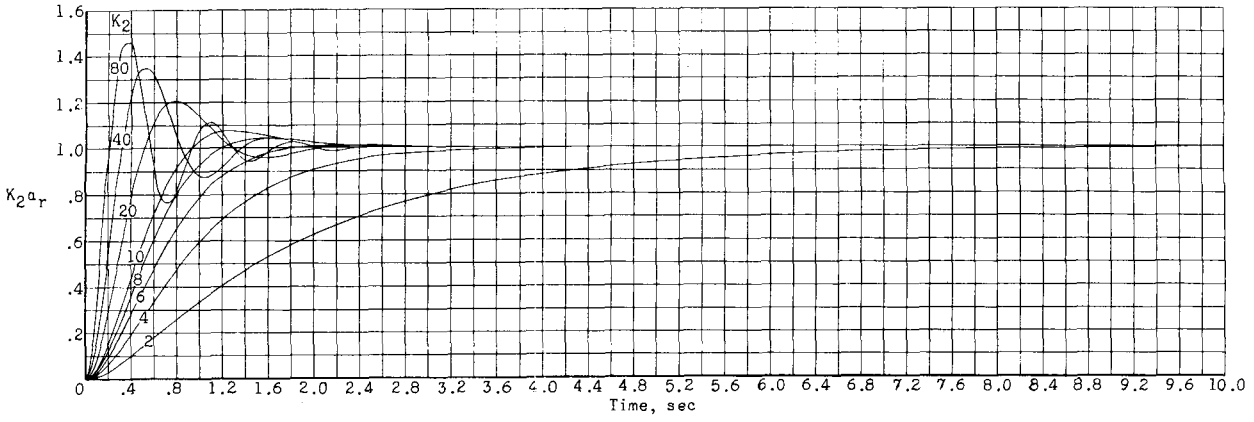

(c) $K_1 = 4.$

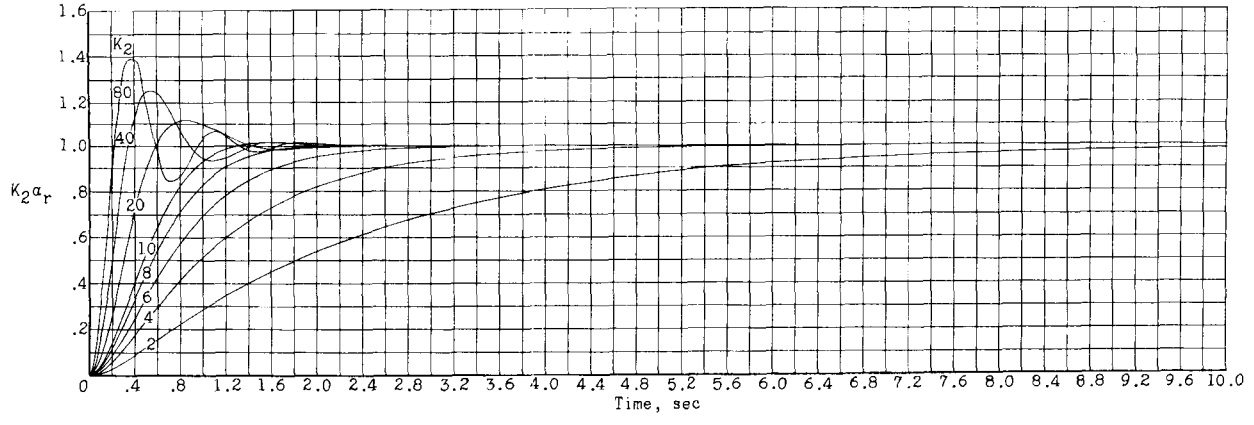

(d) $K_1 = 5.$

Figure 20.- Continued.

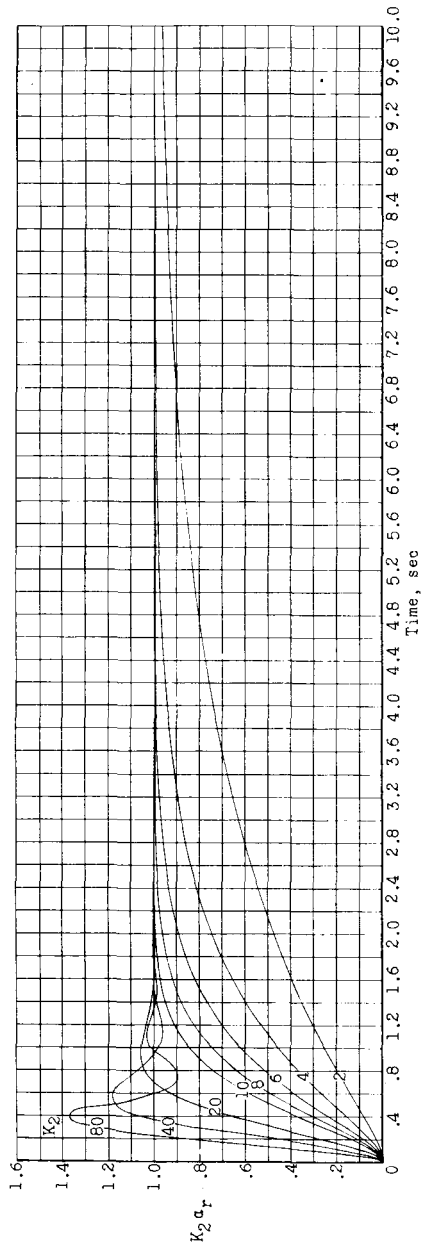

(e) $K_1 = 6$.

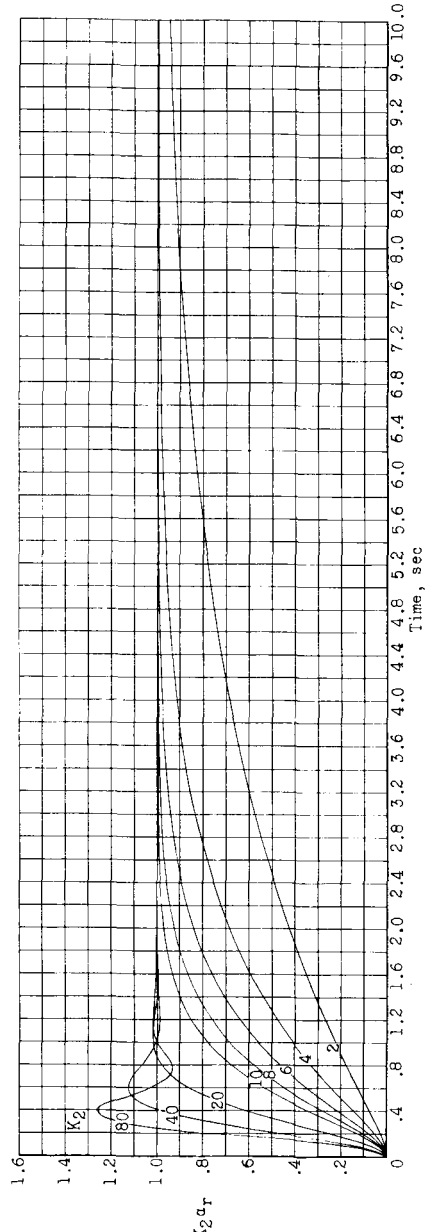

(f) $K_1 = 7$.

Figure 20.- Continued.

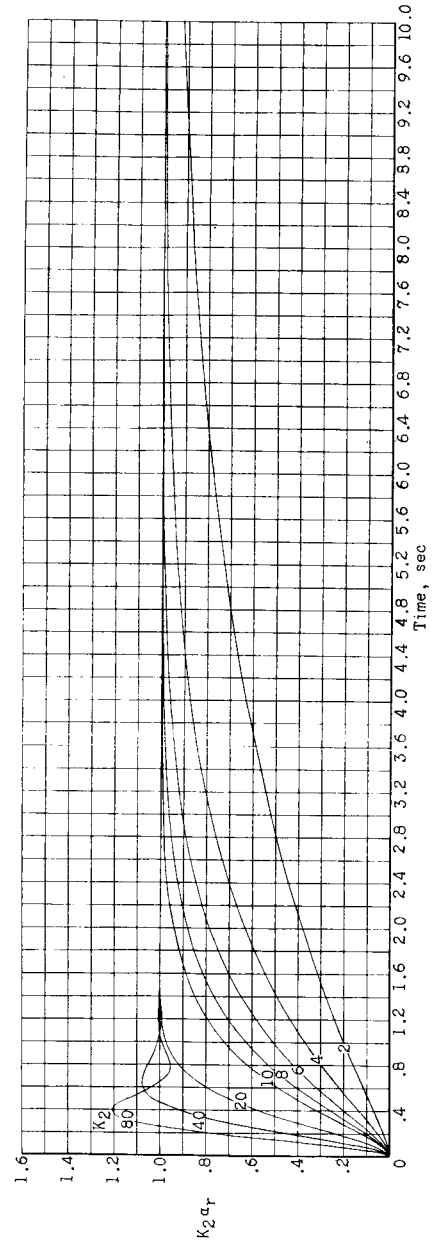

(g) $K_1 = 8$.

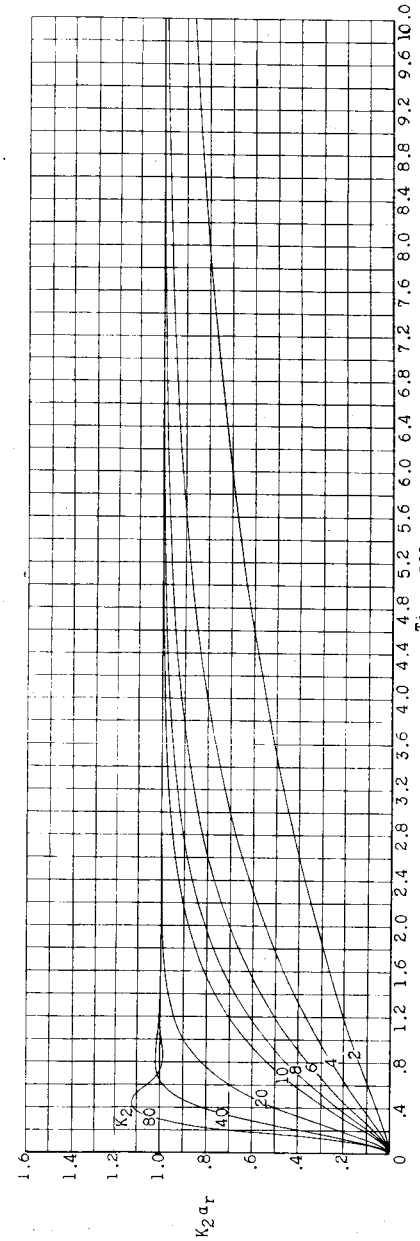

(h) $K_1 = 10$.

Figure 20.- Concluded.

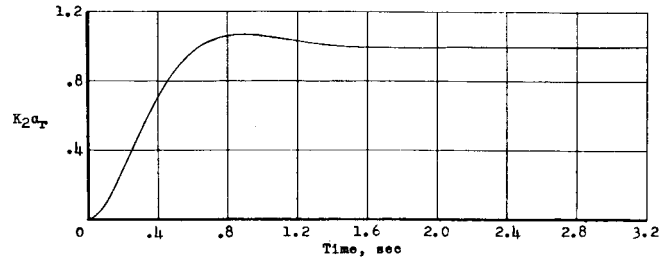

(a) Variation of $K_2\alpha_r$ with time (interpolated from fig. 20(e)). $K_1 \approx 6.0$; $K_2 \approx 21.6$.

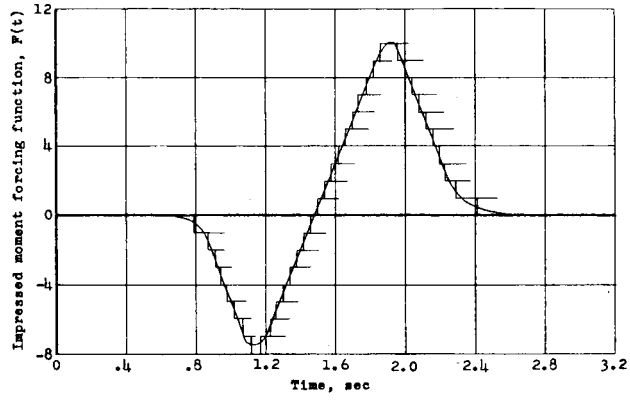

(b) Superposition of F(t) with unit step functions 1(t).

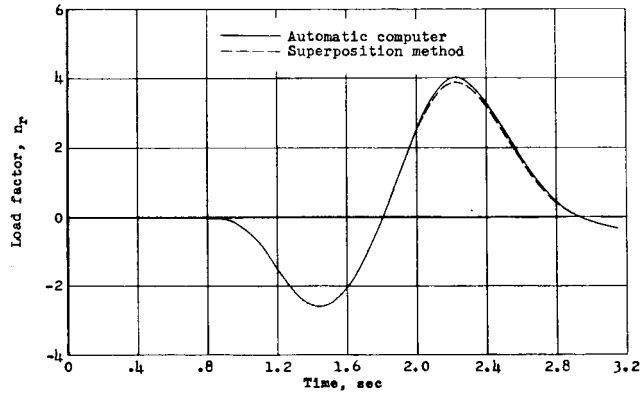

(c) Comparison of calculated airplane load factors.

Figure 21.- Example of applying the derived charts of figure 20 to calculate a load factor due to F(t).